JPRS 77062

24 December 1980

China Report

SCIENCE AND TECHNOLOGY

No. 73

FBIS FOREIGN BROADCAST INFORMATION SERVICE

NOTE

JPRS publications contain information primarily from foreign newspapers, periodicals and books, but also from news agency transmissions and broadcasts. Materials from foreign-language sources are translated; those from English-language sources are transcribed or reprinted, with the original phrasing and other characteristics retained.

Headlines, editorial reports, and material enclosed in brackets [] are supplied by JPRS. Processing indicators such as [Text] or [Excerpt] in the first line of each item, or following the last line of a brief, indicate how the original information was processed. Where no processing indicator is given, the information was summarized or extracted.

Unfamiliar names rendered phonetically or transliterated are enclosed in parentheses. Words or names preceded by a question mark and enclosed in parentheses were not clear in the original but have been supplied as appropriate in context. Other unattributed parenthetical notes within the body of an item originate with the source. Times within items are as given by source.

The contents of this publication in no way represent the policies, views or attitudes of the U.S. Government.

PROCUREMENT OF PUBLICATIONS

JPRS publications may be ordered from the National Technical Information Service, Springfield, Virginia 22161. In ordering, it is recommended that the JPRS number, title, date and author, if applicable, of publication be cited.

Current JPRS publications are announced in Government Reports Announcements issued semi-monthly by the National Technical Information Service, and are listed in the Monthly Catalog of U.S. Government Publications issued by the Superintendent of Documents, U.S. Government Printing Office, Washington, D.C. 20402.

Indexes to this report (by keyword, author, personal names, title and series) are available from Bell & Howell, Old Mansfield Road, Wooster, Ohio 44691.

Correspondence pertaining to matters other than procurement may be addressed to Joint Publications Research Service, 1000 North Glebe Road, Arlington, Virginia 22201.

JPRS 77062

24 December 1980

CHINA REPORT

SCIENCE AND TECHNOLOGY

No. 73

CONTENTS

ABSTRACTS

BUILDING STRUCTURE

GEOLOGY

OCEANOLOGY AND LIMNOLOGY

SEISMOLOGY

SHIPS

APPLIED SCIENCES

SMALL MULTIPLE TERMINAL NETWORK OF DJS-130 COMPUTER ASSEMBLED

Beijing DIANZI KEXUE JISHU [ELECTRONICS SCIENCE AND TECHNOLOGY] in Chinese No 9, 9 Oct 80 pp 30-33

[Article by Fang Cunzheng [2455 1317 2973] of Shanghai Normal University: "Introduction to the Small Multiple Terminal Network of the DJS-130 Computer"]

[Text] General Description

In the past, when we used computers, we followed the method of one user using one computer. This method of a single user occupying one computer did not allow the full utilization of the high speed automatic computational capabilities of the computer. The method is unsuitable for the situation of an ever increasing popularization of the computer. In particular, more and more demands on learning and using computers in teaching and scientific research are being made, therefore it is very necessary to change the method of using computers and to fully utilize the potential efficiency of the computer.

We have assembled a network of small terminals for the DJS-130 computer at school and set up many terminals at places far away from the location of the mainframe machine. In this way, the users can directly use the computer housed at a far distance from their own offices or laboratories. The system as set up at present is shown in Figure 1.

The mainframe DJS-130 has a main memory at present of 20K. The major peripheral equipment in the mainframe computer room is a paper tape puncher and control panel typewriter. The multiplex communicator interface has 4 to 6 terminals.

The terminal equipment can be a five-unit teletypewriter or an eight-unit teletypewriter (such as a pin printer) or it can also be an eight-unit character display. Ordinarily, the terminal equipment of a computer must have a keyboard as a means for input and a printer or a display as a means of output. Because the character display has the advantages of high speed of transmission, low noise and certain editing capabilities, therefore we used the XZX - 1 model eight-unit character display as one of the small multiple terminal network's terminal equipment.

The following is a brief introduction to the problems of multiple terminal processing and long line transmission.

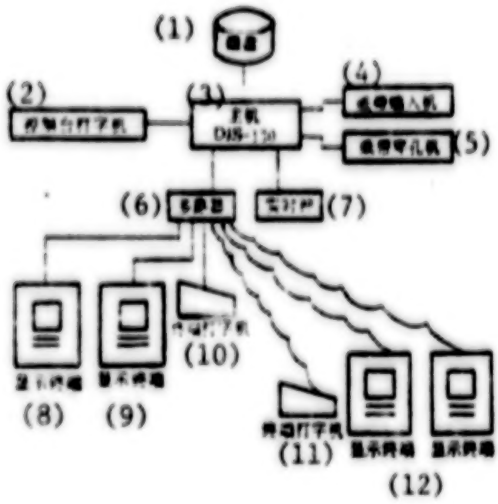

Figure 1.

Key:

(1)	Magnetic disc	(7)	Real time clock
(2)	Control panel typewriter	(8)	Display terminal
(3)	Mainframe	(9)	Display terminal
(4)	Paper tape input device	(10)	Terminal typewriter
(5)	Paper tape puncher	(11)	Terminal typewriter
(6)	Multiplexor	(12)	Display terminal

The Problem of Multiple Terminal Processing

To realize multiple terminal processing, a combination of hardware and software is required.

Each terminal needs two parts, an input (keyboard) and an output (display or printer). Therefore they must each have two interfaces with the computer. One is the receiving unit connected to the keyboard for input of data to the mainframe. The other is the transmitting unit connected to the display or the printer for the mainframe's output of data.

The entire set of multiple terminals is taken as a whole and joined to the interrupt units of each part of the peripheral equipment by queuing via a multiplexor. It occupies one device code (30). Inside the multiplexor, the problem of queuing of the terminals also exists. Their interrupt priorities are determined by the queuing circuits inside the multiplexor. In the mainframe, a method of "device numbering" is used to identify which terminal has requested input and output. Each terminal unit is assigned a "station number." This "device code" is input and output together with the character coded information when executing input and output commands. For the DJS-130 machine, the word length is 16 digits, thus the information for transmitting one word is arranged as follows:

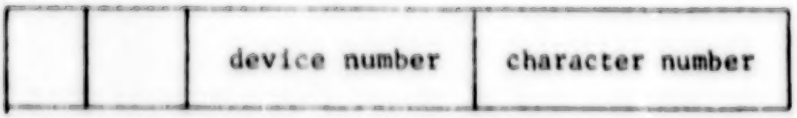

The mainframe uses three input and output transmission commands to exercise control over input and output of the multiplex terminals. One is the input command. The second is the output command. The device code of the multiplexor is (30) and the memory code is AHM. The receiver and transmitter of each terminal have their own "ready" indicator. The "reception ready" indicator and "transmission ready" indicator are also input together with the codes when executing the input command for the mainframe to decide. The input and output commands can also be used to clear these two indicators.

Input command DIAC---, AHM

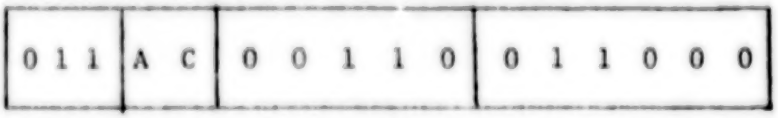

This command processes the input of the character codes. It reads in the terminal interrupt message which is in a reception or transmission readystate and which has received interrupt priority and the "reception ready" indicator of this station number is cleared. The content of the AC full adder being read in is:

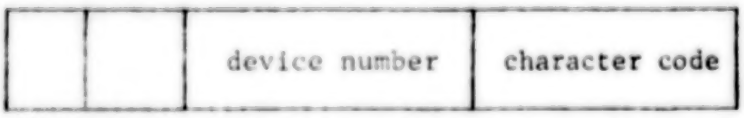

The 0 digit: The "reception ready" indicator is 1, indicating that the terminal represented by the station number shown in the 2nd to 7th digits already has input codes. The input codes are shown by the 8th to 15th digits.

The 1 digit: The "transmission ready" indicator is 1, indicating that the terminal represented by the station number shown in the 2nd to 7th digits already has completed the transmission of codes and is waiting to transmit the next code.

The 2 to 7 digits: They indicate the code of the device which has received the highest priority and which has been set by the "ready" indicator.

The 8 to 15 digits: When the 0 digit is 1, it indicates that a code is received. When the 0 digit is 0, it is void.

Output command DOA---, AHM

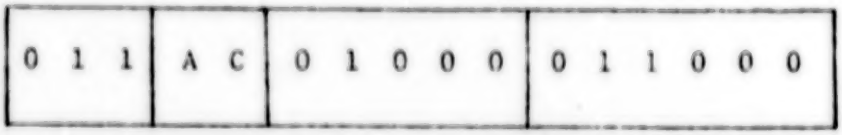

This command processes the output of character codes. It sends the codes to be output from the mainframe to the transmitter of the designated station number and clears the "transmission ready" indicator of the terminal of this station number. As described above, the character code and the designated station number at this time are all in the AC:

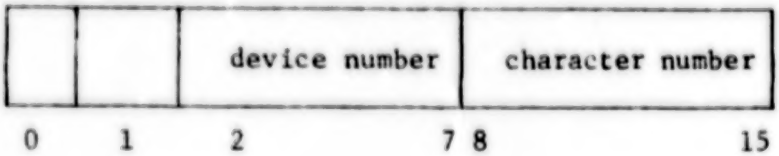

Output command DOB---, AHM

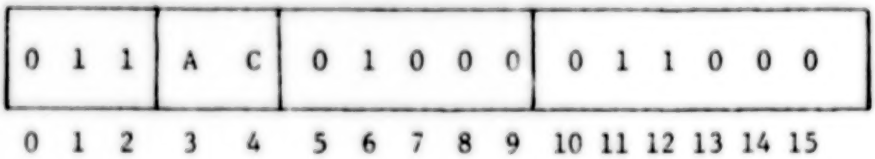

This command clears the "transmission ready" indicator of the terminal, with the station number designated by the 2nd to 7th digits in the AC. It does not execute output of the codes.

Figure 2 is an illustrative block diagram of the logic of the connections of the signals between the multiplexor interfaces and the mainframe and terminal equipment. Its operational process is generally as follows: During input after the keys on the keyboard have been pressed, the receiver shifts the serial codes transmitted by the keyboard digit by digit into the shift register. After the code has been completely shifted into the register, the "reception ready" indicator trigger is set, indicating this shift has been completed. During output after the transmitter has completed shifting the parallel codes sent by the mainframe into the shift register, the serial shift is sent to the printing or display unit. When the shifting of the codes is completed, the "transmission ready" indicator trigger is set. When the "reception ready" or "transmission ready" indicator trigger of any terminal is set, and under the control of the status trigger, an interrupt request ZDQQ signal is sent to the mainframe. At this time the entire multiplexor makes the request to the mainframe as a whole unit. After the mainframe responds to the interrupt signal, a ZDXW signal is sent and when it receives an interrupt priority by queuing in the multiplexor, the device code (30) is sent to the mainframe, via the input bus MX_R. Thus, the mainframe enters into a service routine of executing the interrupt signals of the multiplexor.

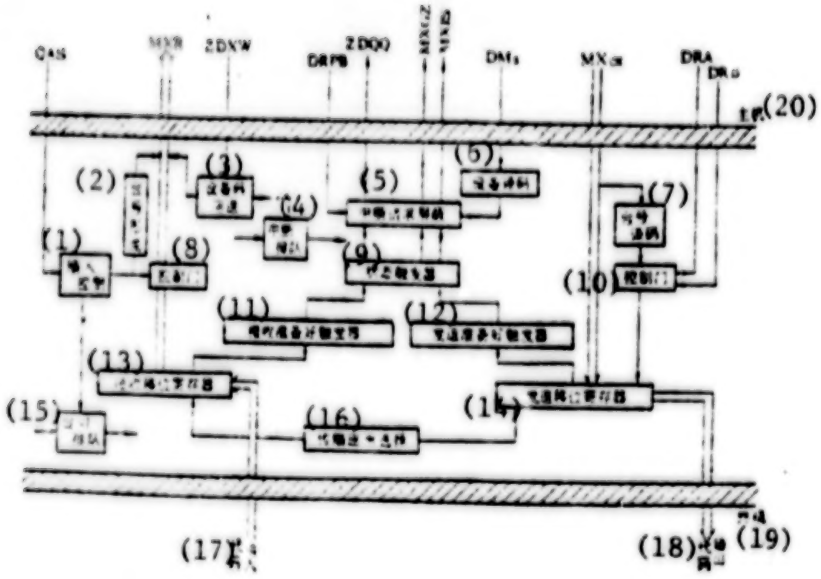

Figure 2.

Key:

(1) Input control
(2) Formation of station number
(3) Sending back equipment (device) code
(4) Interrupt queuing
(5) Interrupt request masking
(6) Device decoding
(7) Station number decoding
(8) Control gate
(9) Status trigger
(10) Control gate
(11) Reception ready trigger
(12) Transmission ready trigger
(13) Reception shift register
(14) Transmission shift register
(15) Queuing between stations
(16) Transmission speed selection
(17) Code input
(18) Code input
(19) Terminal
(20) Mainframe

The illustrative block diagram of interrupt processing is shown in Figure 3. First, the DIAC---, AHM command sends the interrupt signal in the receiver of the terminal that has made an interrupt request and that has obtained interrupt priority via the input bus MX_R into the mainframe and clears the "reception ready" indicator trigger in that terminal. Then the 0 digit of the message is recognized and taken in by the mainframe. If the 0 digit is 1, then reception ready is indicated. The mainframe thus knows by the device code taken in which terminal has input the character and will carry out the corresponding processing of the input character codes. After the "reception ready" indicator has been cleared, the initial state is restored to wait for the input of the next character. If the 1 digit is 1, transmission ready is indicated. Thus the mainframe uses the DOBO AHM command to clear the "transmission ready" indicator and enters into transmission processing AHOUT. When the mainframe wants

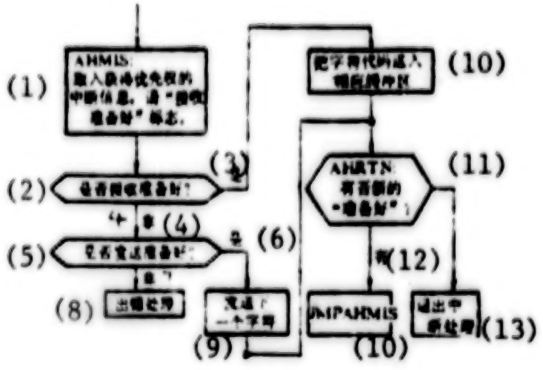

Figure 3

Key:

(1) AHMIS: Accessing interrupt signals having priority, request "reception ready" signal
(2) Whether reception ready or not?
(3) Yes
(4) No
(5) Whether transmission ready or not?
(6) Yes
(7) No
(8) Processing of error
(9) Sending the next character
(10) Sending character codes into corresponding buffer zone
(11) AHRTN: Are there any new "ready"?
(12) Yes
(13) Withdraw from interrupt processing

that terminal to execute output operations, the mainframe sends out a DOA---, AHM command, the device code in the corresponding accumulator of the mainframe is sent to the multiplexor via the output bus MX_{cx2-7} and transmits the entry signal to send the code to the output into the shift register via the bus MX_{cx8-15}. After each digit of the code has been shifted out, the "transmission ready" indicator is set again. The above process is thus repeated. After completion of one receiving or transmitting process, the program enters a return process AHRTN, a check is conducted to see if there are any other interrupt requests from other terminals. If there is, then an AHMIS is executed. If there are no new requests, the program withdraws from interrupt processing.

The work concerning the multiplexor interfaces has been described in an article entitled "A Plan for Multiplex Terminal Interfaces of the DJS-130 Computer" published in the fourth issue of 1978 of "Electronics Science and Technology."

After the plan for the hardware has been determined, the problem of the method of connecting the terminal user and the system is solved only. To enable many users to realize on line operation simultaneously, there must be software to

realize management of and time sharing for each user. At present we have installed a multiple user expanded BASIC magnetic disc on the small terminal network. This system utilizes time sharing to manage the operations of the users of multiple terminals. A maximum of 16 users can be allowed to use the expanded BASIC language to solve problems on their own terminal equipment simultaneously. This interpretive program itself takes up 10K of main memory and the remaining main memory area is distributed to each terminal user allowed to operate the machine as working area. In this way, if the main memory has 32K and 16 users are allowed to operate the machine, then each user can be given about 1.4K of the main memory area. As regards time in realizing time sharing, this system divides time into several time rules. Each time rule is 160mS. The mainframe provides time to each terminal user to use in turn according to the time rules and executes the programs currently being executed by the user. Using such time rules, the system can respond to the requests of each end user more effectively. When all 16 users work on line simultaneously, the delay between two runs of a user's program is about 2.5 seconds. In this way, each user feels as if he is using the mainframe for computations alone within his own alloted time rule and utilizing a shared systems program at his own fixed place of work.

The installation of a real time clock is to provide the system with a time standard. The real time clock sends one interrupt request to the mainframe every 10 seconds to systematically count time. The system records the time each user uses the mainframe and the peripheral equipment according to the time signals provided by the real time clock. It then produces the 160mS time rule to implement management of time sharing for each user. When there is a far away terminal, the call signals of the far away user can also be inquired and answered at fixed intervals.

Let us talk about the problem of time estimation for the mainframe to respond to interrupt signals when the system is carryout out multiple terminal processing. We assume that each interrupt service program has an average of 50 commands and each command would require 5 μS of time, then processing one interrupt signal requires 50 X 5 μS = 250 μS. When all 16 terminals are connected, one round of processing all input and output interrupt requests requires a total of 2 X 16 X 250 μS = 8mS. For the keyboard input, the time interval of pressing 2 keys is about 250mS. This is sufficient to process the interrupt signals of 16 terminals. For the output, if a transmission speed of 1200 baud is used, the shiting of each digit of a character requires about 0.83 mS X 11 = 9.13 mS. Even with the addition of other control codes, the time is sufficient to process the interrupt requests of 16 terminals, and the work efficiency of the terminal equipment will not be lowered too much. Observation of actual use shows that when the output is higher than 1200 baud, the output will not realize a faster speed because of the inherent limitations of the processing capabilities of the mainframe itself. Therefore, this system is best suited for a transmission speed of below 1200 baud. When the system reschedules the peripheral equipment, processing at each terminal clearly slows down.

The Problem of Long Line Transmission

For lengths longer than several dozen meters, connecting the terminal equipment to the computer with a double strand wire for each digit when the parallel code transmission method is used is obviously very unsuitable. Therefore the serial

code transmission method is generally used, such as the teletypewriter and the character display. The terminal and the computer are connected by an asynchronous operational mode, i.e., a start-stop method. The standard input and output equipment with keyboard uses an 11-digit coding of each character. One digit is the startup digit and 8 digits are message digits (of which 1 digit is parity number) and 2 digits are stop bits.

When using serial code transmission, generally only two signal lines are sufficient between the terminal and the mainframe. One line is the code signal line for transmission from the terminal to the mainframe. The other is the code signal line for transmission from the mainframe to the terminal. Some terminal printers that require an additional control signal line such as the DZM180KSR model pin printer poses a 256 unit buffer memory. When this buffer memory is temporarily full, a control signal has to be transmitted to stop the mainframe from sending more codes to the printer. These transmission lines all use double strand wires. For far away terminals over 100 meters distant we set up special transmission lines. These lines use ordinary 2 x 42/0.15 polyethylene insulated electric wire as the double strand wires. The transmission voltage on the line generally should be 15 to 20 volts, the line current is about 20mA. According to the standards of the computer, such an electrical balance of signals is very large, but there are great advantages to the transmission function. It enables the terminal to resist the effects of electrical resistance of more than several hundred meters of wire while the accuracy of data transmission is not affected. This is because smaller noise or interfering voltage will not affect the code signals being transmitted. Conversely, if a lower signal electrical balance is used, such as 2 to 3 volts, interfering signals may completely destroy data transmission. Another advantage is that this type of circuits can provide a constant source of flow. It does not depend on long wire resistors. This type of circuits is often called "20mA current loop circuits." Figure 4 illustrates the principle of conversion between the interfaces of the computer and the "20mA current loop circuit."

To overcome common mode interference, the best method is to electrically insulate the interface between the transmission line and the computer completely. Good results can be obtained by using photoelectric couplers. Photoelectric coupling involves putting an emitting diode and a silicon photoelectric triode together. Code transmission is realized by light. The coupling between input and output has only 0.5 to 2pF of capacitance. The largest data transmission rate is determined by the frequency response of the photoelectric triode (which can reach several dozen to over 100 kilohertz). Such a frequency response is entirely sufficient for connecting the keyboard, printer or display screen and the computer. We have used the 3EDK62 model photoelectric coupler. Its circuit is illustrated in Figure 5.

After taking the above measures, the distance between the computer and the terminal equipment can be as distant as over 2 kilometers. At present, we have set up three relatively distant terminals in the school for use by the physics, chemistry and biology departments. Via the long line, the connecting circuit between the computer and the terminal equipment is shown in Figure 6.

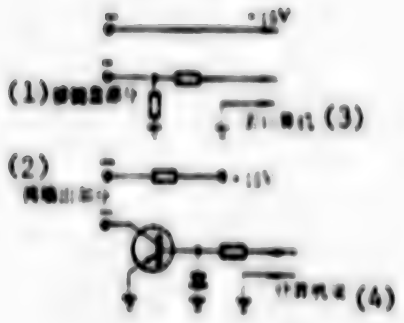

Figure 4

Key:
(1) Connected to the keyboard
(2) Connected to the output
(3) Goes to computer
(4) Coming from the computer

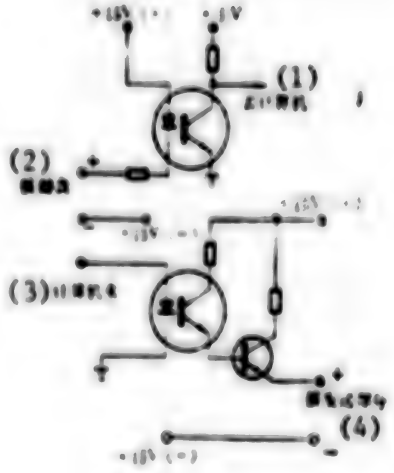

Figure 5

Key:
(1) Goes to computer
(2) Connected to keyboard
(3) Coming from computer
(4) Connected to transmission

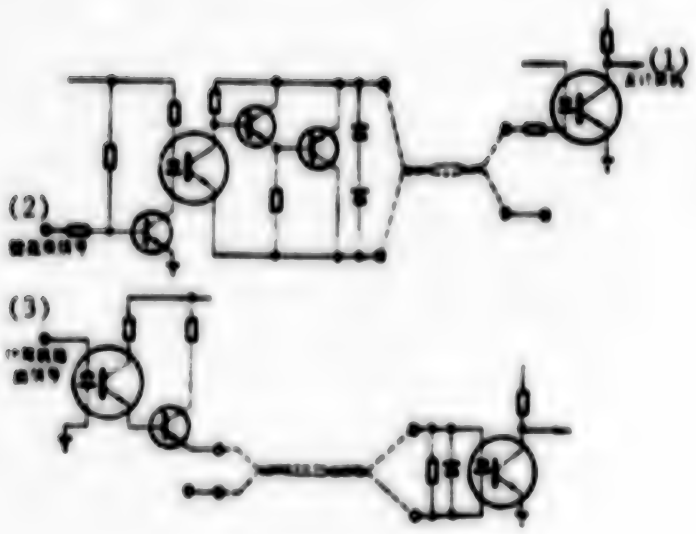

Figure 6.

Key:
(1) Goes to computer (2) Signal from keyboard (3) Output signal from computer

The success of the experiment of the small multiple terminal network gave us the opportunity for a preliminary attempt in the realization of a computer network and definite material preparations have been made for further work. At present, we have also added a magnetic disc storage onto this system and are preparing corresponding software and other hardware to launch further work.

9296
CSO: 8111/0196

DJS-130 COMPUTER QUALITY EVALUATION RESULTS REVEALED

Beijing DIANZI KEXUE JISHU [ELECTRONICS SCIENCE AND TECHNOLOGY] in Chinese No 9, 9 Oct 80 p 29

[Article by correspondent of the National Computer Industry Administration: "National DJS-130 Computer Quality Evaluation and Comparison Results Are Revealed"]

[Text] Our nation's first DJS-130 computer quality evaluation and comparison event was held. After 47 days of evaluation and comparison, the results were made public in Tianjin on 15 July 1980. The Shanghai Computer Plant, the Suzhou Computer Plant, the Tianjin Radio Plant No 2, were awarded first prize. The Weifang Computer Plant No 6, Changzhou Radio Plant No 2, Yunnan Electronics Equipment Plant received praise in the evaluation and comparison of learning and emulation.

A total of 14 machines from 7 production facilities in the 5 provinces and cities of Beijing, Tianjin, Shanghai, Jiangsu and Shandong participated in the overall evaluation and comparison. Four production facilities of the four provinces of Shanxi, Jiangsu, Henan and Yunnan participated in the evaluation and comparison for learning and emulation. The emphasis of this evaluation and comparison show was to inspect reliability of the machines. The items of evaluation and comparison were stability experiment of continuous operation for 720 hours, inspection of function, inspection of capabilities of forming whole systems, inspection of technical structure and inspection of cost. In the evaluation and comparison, 3 machines of 3 plants operated without malfunction continuously for 1,000 hours and they were turned off manually. Six other machines continuously operated for 500 hours to over 800 hours. The machines that participated in the evaluation and comparison basically all passed the inspection of function.

The results of this evaluation and comparison event show that the domestically produced DJS-130 computer's reliability, stability and capability for forming whole systems visibly improved and the cost dropped, reflecting progress over the past several years in our nation's computer industry.

9296
CSO: 8111/0196

APPLIED SCIENCES

TYPES OF DATA DISPLAY SYSTEMS OUTLINED

Beijing DIANZI KEXUE JISHU [ELECTRONICS SCIENCE AND TECHNOLOGY] in Chinese No 9, 9 Oct 80 pp 40-41

[Article by Cheng Changfu [4453 7022 4395]: "Electron Beam Tube and Computer Technology"]

[Text] Since 1960, a brand new technological field in peripheral equipment that further enhanced the functions of computers rapidly developed--data display systems. They include character display, graphic display and composite display of text and background graphics. The displays were also equipped with such electronic input devices as voltage pen, photosensitive pen and word recognition devices. Data display systems made conversation between man and machine more graphic and convenient.

Main Display Devices in Data Display Systems

The main display devices of the display of a computer are the various types of cathode ray tubes (abbreviated CRT). There are many types as described in the following:

1. To enable the deflection component to simultaneously have the two functions of registration and character generation, a double deflection CRT is used. It can be assembled in two ways. The first is an electromagnet-electromagnet type. The other is the electromagnet-static type. When using the electromagnet-electromagnet type, registration on the fluorescent screen is realized by a coil having a high electrical sensitivity. Character generation is realized by a coil that has a low electrical sensitivity so that the scanning response speed of characters can be increased. When the electromagnet-static deflection is used, electromagnet deflection is used to realize registration while static deflection is used to realize character generation.

2. The multiple electron gun that can display two or more messages and data simultaneously. The static dual gun's typical application is as follows. One electron gun is used to generate radar data. The other electron gun is used to generate computer data.

3. To increase the capacity of the message, a color CRT is used. Fluorescent powder of various colors is used to display different data that is to be differentiated so that the various data zones are clearly different. There are two

types of color CRT: one is a cathode shielded color image reproducer. The other type is a voltage penetration type multicolor image producer. The voltage penetration type fluorescent screen also includes two types, a wrapped fluorescent screen with multiple colored layers and a lined fluorescent screen. There is another type of current sensitive multicolor image reproducer under research. The structure of the voltage penetration type multicolor image reproducer is much simpler than that of the cathode shielded color image reproducer. It uses only one electron gun to achieve color displays. When the high screen voltage is switched over at high speed within a definite range, electron beams of different acceleration energy penetrate and excite the fluorescent powder to emit many different colors of red, orange, yellow and green and afterglow. There are many varieties of voltage penetration type multicolor image reproducers abroad. The full screen resolution of this type of electron tubes can generally reach 1,600 lines, brightness can reach 150 Nit. When the high screen voltage is switched over at 6 kilovolts to 14 kilovolts, 4 to 5 colors can be obtained or the afterglow can be changed.

4. High resolution CRT is suitable for photographically recording data or as fly-point scanning of a light source (such as a word recognition device). This type includes the fiber optics surface board CRT. Because a fiber optics surface board is used as the surface board of the fluorescent screen, its transparency is high, its light gathering ability (numerical aperture) is large and image distortion is small. The optical fiber used to make the surface board has a diameter of from 5 to 10 micrometers each. This type of electron tubes can scan light spots of several micrometers to about 20 micrometers. There is a type of flat line scanning tube encased in a glass shell. Its optical fiber surface board is a rectangular narrow band type. It records one line of data photographically each time.

5. To overcome the shortcoming of short afterglow of the ordinary CRT, the computer uses a direct view storage tube (abbreviated DVST). This type of electron tube has a longer-storage time under strong brightness (generally several hundred times or more than the brightness of ordinary display tubes) and the afterglow can be changed. The advantage of the DVST data display is that it need not interrupt the computer frequently because of renewal of data. To selectively clear partial data from the fluorescent screen a selective clearing or multiple state DVST can be developed. The storage method of DVST generally can use a half tone (gray scale type) or a bistable (black and white type) mode of operation. The bistable electron tube is mainly used for wave form display while the half tone is used where a gray scale is required. The DVST is a kind of structurally complex electron beam tube. It generally consists of four parts, a gathering network--energy storage target network--fluorescent screen, correction system, reading electron gun and a recording electron gun. The ordinary recording speed can reach several dozen thousand meters to several million meters per second (if the so-called projection type energy storage CRT made from a post magnification electron lens is used, the recording speed will be higher). The saturation brightness of the fluorescent screen can reach 4,000 meters lambert above (the saturation brightness of the cathode shielded color image reproducer is generally above 100 meters-lambert). The effective image time or called the changeable afterglow

can reach 10 seconds to 1 hour. DVST's resolution and the line density of the energy storage target net are closely related, generally the diameter of the light spot can reach 0.25 millimeter to 0.75 millimeter. DVST message storage can last from several days to about 1 week.

6. Single gun or multiple gun electrical output storage tube and the scan switchover storage tube can store input data with one speed while the other speed is used to provide electrical signal output.

7. The electron gun of the character code tube formed in the character tube is of the dual cross type electron gun. Its major difference from other CRT is that in its electron optics system, an etched and hollowed out thin metallic sheet with numbers and symbols on it called the "character font" is in its electron optics system in the character code tube.

Display Terminals of the Computer

The data display terminals of computers are mostly rectangular screens. In general, P19 (orange red) and P39 (green) long afterglo fluorescent powder are used because they have a low frequency of glare and they are easy on the naked eye. To increase the message capacity within definite dimensions of the screen, the resolution of the electron gun must be further increased. Japan's Matsushita Company produced the 340BAB39 model data display tube using P39 fluorescent powder on its fluorescent screen. The screen is only 14 inches but the maximum resolution of its static focus electron gun can be as high as 1800 lines. Generally this type of electron tubes uses electromagnetic deflection. Because the comprehensive (trend) display of the activity on the computer terminal operates in a random scanning mode, the angle of deflection should not be too large to reduce deflection power and deflection coil's electrical sensitivity and to increase the rate of deflection response. It is generally 40° to 70°. This is because an overly large deflection angle will cause nonlinear distortion and deflection focus out. To assure the high clarity and high quality of the image on the whole screen, it is hoped that even large screen data display tubes have a small deflection angle. For example, the deflection angle of the 9-inch dim light spot tube manufactured by Britain's Ferranti Company is only 40°. The deflection angle of the 5-inch high resolution tube of the Sylvania Company of the United States is 50°. When consideration is given to the fast deflection response speed and the conservative deflection power of the static deflection oscilloscope, the development of large screen rectangular oscilloscopes to be used as data display tubes is a direction.

The terminal of a large computer can be fitted with many display heads via appropriate interfaces. This can fully develop the efficiency of the machine. The block diagram of the IBM2250 display developed by IBM of the United States is shown in the diagram. It operates jointly with the IBM2840-2 model display control to produce data display (including letters, numerals and graphs). It uses a 21-inch double reflection type CRT with an effective viewing area of 12 inches X 12 inches as a display device. The CRT fluorescent screen uses 1024 X 1024 matrix of fixed points.

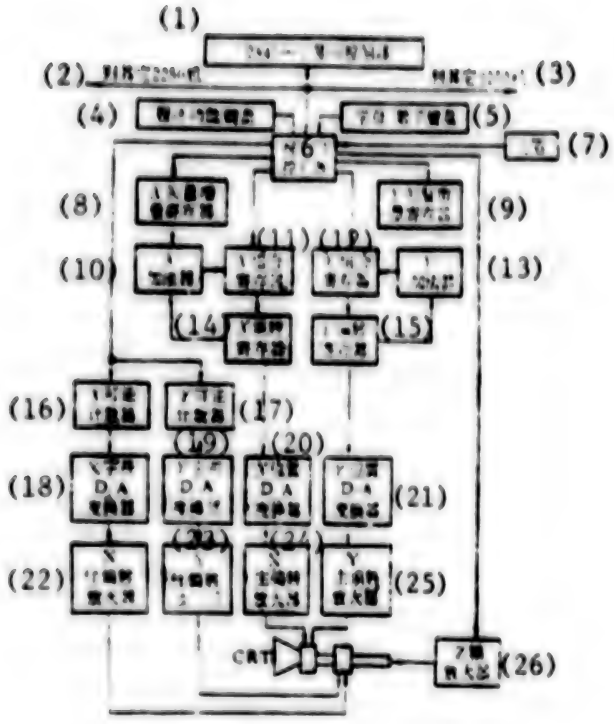

IBM 2250 display block diagram

Key:

(1) 2481-1 display controller
(2) To other 2250 machines
(3) To other 2250 machines
(4) Program function keyboard
(5) Alphanumeric keyboard
(6) Interface controller
(7) Photopen
(8) X vector increment register
(9) Y vector increment register
(10) X adder
(11) X assembly register
(12) Y assembly register
(13) Y adder
(14) X deflection register
(15) Y deflection register
(16) X reversible counter
(17) Y reversible counter
(18) X character D/A transformer
(19) Y character D/A transformer
(20) X position D/A transformer
(21) Y position D/A transformer
(22) X auxiliary transform magnifier
(23) Y auxiliary transform magnifier
(24) X main transform magnifier
(25) Y main transform magnifier
(26) Z axis magnifier

The technique of producing characters is realized by the use of a reversible counter of a pair of X and Y character coordinates to drive a D/A converter. The character storage has 63 standard characters and any stroke combinations suitable to the X, Y character coordinates system can be displayed under the control of the computer. The IBM2250 display is also equipped with a photopen.

The photopen data display is the result of successful application of CRT and photoelectric equipment in computer technology. It has greatly promoted the development of computer technology. To develop more perfect photopen data display systems, CRT with strong brightness and a high message capacity must continue to be developed. The high resolution display tube and the multicolor display tube all have one purpose, to increase the message capacity of the CRT. CRT of a high message capacity has a bright future for broad applications in modern computer technology. The need for data display CRT by the computer will be greater and greater. In the United States, the production of computers with data display CRT in 1978 was about 800,000 units. The degree of popularization of data display CRT will gradually catch up with the image reproducing tubes for television sets.

9296
CSO: 8111/0196

RECOVERY TECHNIQUES OF IONIZATION ADDITIVES IN MHD GENERATION DESCRIBED

Nanjing NANJING GONGXUEYUAN XUEBAO [JOURNAL OF NANJING INSTITUTE OF TECHNOLOGY] in Chinese No 3, Sep 79, pp 82-88

[Article by Lan Jixiang [5663 6060 7449], Zhu Jiazheng [2612 0502 1767], Xu Jianjun [1776 1696 6511], Zhang Xiafu [1728 7209 1381] and Dai Jinmei [2071 6855 1188] of the Research Institute of the Nanjing Chemical Industry Company: "Recovery Techniques of Ionization Additives in Magnetic Hydrodynamic Generation"]

[Text] Abstract

This article describes foreign experimental research in the technique of low temperature recovery of ionization additives in magnetic hydrodynamic generation. It introduces the process, equipment, operating conditions and the index of purification obtained in recovery of seeds (ionization additives) washed in solution of the "spray cup absorber-double aperture bubble tower-venturi tube" system mounted on the simulation machine group JS-1 of the Nanjing Engineering Academy. The article also introduces the situation of experiments on the wet electrostatic dust precipitator. At the same time, it points out the practical application of the solubility diagram in the K_2CO_3 - $KHCO_3$ - K_2SO_4 - H_2O quaternary system.

I. Foreword

In the direct conversion of heat to electricity in magnetic hydrodynamic generation, realization of thermal ionization at a temperature which specific materials can bear and which can be reached by the heater requires the addition of alkaline metallic elements of low ionization potentials such as cesium and potassium (called "seeds" or ionization additives), thus giving the burning gas sufficient electrical conductance. Ordinarily, alkaline metallic salts are used as additives. The amount of alkaline metallic elements added is about 1 percent of the weight of the electrically conducting burning gas.[1]

In the joint circulation of magnetic hydrodynamic-steam power, when potassium carbonate (K_2CO_3) is used as an additive and injected into the burning chamber at 2500°C as a solution, K_2CO_3 gasifies, decomposes and ionizes to produce potassium ions (K^+). They pass through the channels of electricity generation into the steam generator. As the temperature continues to drop, K_2CO_3 is formed

step by step. At 1300°K to 1500°K, it begins to condense and forms highly scattered K_2CO_3 particles. The average diameter of the particles is 0.1 to 0.2 μ.[2] When sulphur containing fuel is used, the fuel is desulfurized and K_2SO_4 is formed. These particles produce a definite condensation in the steam generator and partially settle on the heat exchange surface. Smoke enters the recovery system before it enters the atmosphere so that the restored ionization additives and K_2SO_4 produced by chemical reaction in the smoke are recovered.

The recovery rate of the additives must satisfy the demands of economic guidelines and environmental health guidelines at the same time. Because the demands of economic guidelines are higher than the environmental health guidelines, the allowable loss by exhaust should be determined by the electrical generation equipment and technology. If the allowable loss of potassium additive is equivalent to 1 percent of the loss of fuel or equivalent to a reduction of electrical generation by 0.5 percent, generally the total recovery rate should reach above 99 percent.[2] When using cesium additive, the loss should be even lower. The joint magnetic hydrodynamic-steam power station must recover the additives very efficiently and must regenerate them for recycling so that the operation of the power station can be maintained at a highly economical level and at a low level of pollution.

II. General Description of Research Abroad

Because the additives in smoke are submicroscopic condensed powdery dust and because of some special demands of magnetic hydrodynamic generation, the recovery of additives has become an important research topic. In the research of magnetic hydrodynamic power generation abroad, many studies have been conducted in the three possible recovery methods using gas filtration, washing by solution and by the electrostatic precipitator.[2,3,4] The High Temperature Research Institute of the Soviet Academy of Sciences completed construction of the y-02 simulation equipment with a flow of 1 kilogram/second in 1967. A fiber filter of filter area of 112 meters^2 composed of 4 filtering units was built. Detailed experiments on operating conditions and filter media were conducted. When the specific load is 0.7 to 1.0 meters^3/ meter^2 · minute, and the degree of vacuum of the system is maintained at 50 kilonewtons/meter^2, the dust content at the exit can reach 1 milligram/meter^3. Dust recovery operation must be conducted under a high resistance drop and a higher exhaust temperature (> 200°C). The y-02 equipment also has a bubble tower with two layers of sieves and a so-called "turbulent flow washer" composed of venturi tubes. They form an ionization additives extraction system. The speed in the venturi tube is 60 to 160 meters/second. When the dust content at the entrance is 5 grams/meter^3, and the resistance drop is 15 kilonewtons/meter^2, the dust content at the exit is 0.2 gram/meter^3. When the resistance drop increases to 20 kilonewtons/meter^2, the dust content at the exit can reach 0.1 gram/meter^3. The experiments also showed that the degree of conversion of K_2CO_3 in the extracted liquid to $KHCO_3$ varies with the concentration of the solution. The research achievements of the "turbulent flow washer" on the y-02 has already been used for enlarged design. An ionization additives recovery system composed of a bubble tower, variable rectangular section venturi tube and the round section venturi tube began operation on the y-25 equipment for the industrial magnetic hydrodynamic power generation experiment in 1971 (flow of

50 kilograms/second). The Soviet High Temperature Research Institute conducted a wet electrostatic dust precipitation experiment on the y-02 equipment after conducting gas filtration and solution washing experiments. The length of the electrodes of the wet board type electrostatic dust precipitator was 0.8 meter, the flow was 200 grams/second, the flow velocity was 0.5 to 0.7 meter/second, the operating voltage was 50 kilovolts, the recovery rate reached 93 percent. According to reports, the y-25 equipment is also being designed for equipping it with an electrostatic dust precipitator. England, in her early research on magnetic hydrodynamic power generation, conducted experiments on the dry single tube electrostatic dust precipitator at the Central Electrical Appliances Test Laboratory using K_2SO_4 as the additive. Japan's Electronics Technology General Research Institute developed the magnetic hydrodynamic-thermal power generation system for long periods of experiments--the No 6 generator. A dry electrostatic dust precipitator was installed in front of the exhaust and a very high efficiency was achieved.

III. Experimental Research and Results

Experimental research[5,6] on the recovery of ionization additives in power generation by the wet electrostatic dust precipitator and solution washing was conducted on the JS-1 generator group of the simulation experiment of magnetic hydrodynamic power generation at the Nanjing Engineering Academy. The flow chart of the solution washing experiment using the spray cup absorber-double aperture bubble tower-venturi tube system with the venturi tube as the centerpiece is shown in Figure 1.

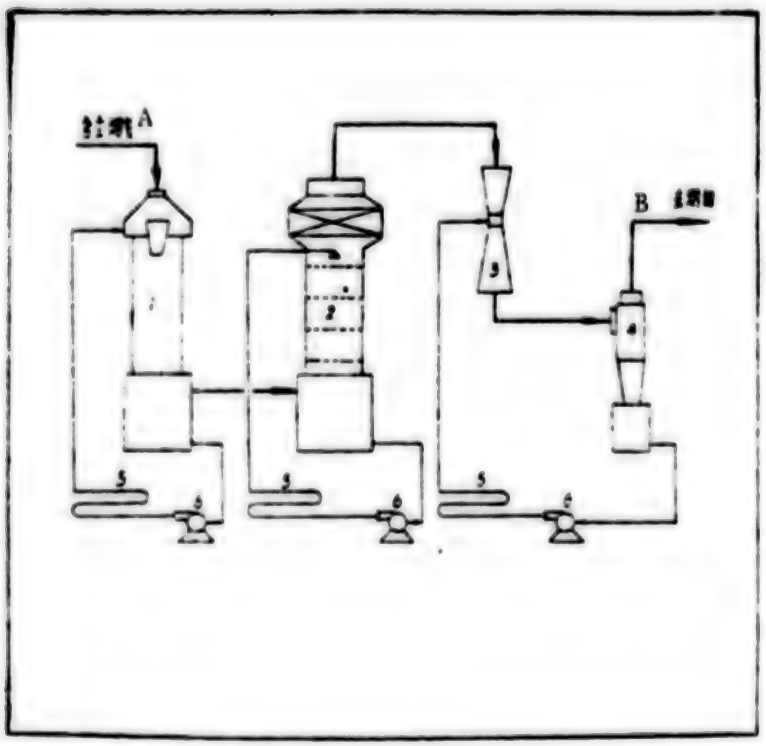

Key:
A Dust containing smoke
B Exhaust smoke stack

1. Spray cub absorber
2. Double aperture bubble tower
3. Venturi tube
4. Whirlpool bubble remover
5. Heat transformer
6. Pump

Figure 1. Flow chart of retrieval experiment of the solution washing method

Smoke containing potassium carbonate forms an overflowing liquid film from the circulating liquid on the wall of the spray cup. At the bottom of the cup smoke gushes out at a velocity of 25 meters/second, causing the liquid film to atomize and enter the absorption zone. Then through a separation zone, it enters bubble tower 2 composed of double aperture sieve boards in structure from the b ttom. At the top, the first sieve board is a single aperture sieve board which serves to distribute the liquid. The last three sieve boards are double aperture sieves. The designed speed of flow in the tower is 1.8 meters/second, and the speed through the aperture is 9 to 10 meters/second. The gas and the liquid manifest throughflow and complex flow movements on the sieve boards, realizing full contact between the gas and the liquid. At the top of the bubble tower is a bubble removal layer that fills the magnetic ring. After removing the bubbles, the smoke enters the contraction section of the venturi tube from the top. When it passes through the tube at a high speed of 60 to 120 meters/second, the alkaline solution being sprayed into the tube from all sides fully atomizes, making the dust particles wet and the dust particles condense fully in the dispersion tube. After the gas and the liquid are separated in the whirlpool separator 4, smoke that is highly purified is exhausted from the smoke stack. The solution in the three installations are circulated by pump 6. Changing the amount of cooling water in the heat exchanger 5 can control the temperature of the circulating alkaline solution. The alkaline solution circulation trough of each equipment has an alkaline tolerant coat of cyclic oxyfuran.

The solution washing recovery experiment was conducted in two ways: (1) The experiment was conducted along with the long period experiment of power generation by the power generator group. At this time, water is used to cool the channels and the smoke is sent into the recovery system. (2) The experiment was conducted by simulating the gas distribution under smoke exhaust conditions in actual power plants. At this time, the hot air of the heat storage furnace is not used for burning, but the burning temperature must be kept at or above 1600°C so that the liquid additive can fully gasify. Under given operating conditions, after the system is running stably, a sample is taken at each point every half hour. The samples of dust contained in the smoke are taken by a jet sampling gun and measured by a flame brightness meter, K^+.[6] This method avoids precipitation of dust particles on the sampling tube and can determine the total amount of potassium. Partial experimental data are listed in Table 1 and Table 2.

It can be seen from Table 1 and Table 2 that as the resistance loss of the system rises, the recovery rate visibly increases. When the resistance loss of the venturi tube reaches or surpasses the designated value (850 millimeters of water) a very low content of dust in the exhausted smoke can be obtained. The venturi tube is very effective in condensing and collecting fine powdery dust. The experiment shows that the following major operational parametric values should be realized:

	Velocity of gas meter/second	Liquid and gas ratio meter^3/1000 meter^3
Spray cup absorber	25	4
Double aperture bubble tower	1.5 - 1.8	3 - 4
Venturi tube	⩾ 96	0.9 - 1.1

Table 1. Table of Data of Retrieval of Additives in Systematic Power Generation

(1)烟气温度 ℃				(2)系统阻力 毫米水柱	(3)烟气含尘 克K·/米³		(4)碱液浓度 %			(5)净化度 %
(6)进入烟气	(7)喷杯后	泡沫塔后 (8)	排烟 (9)		进入烟气 (10)	排烟 (11)	喷杯 (12)	泡沫塔 (13)	文氏管 (14)	
370	125	62	60	542	9.2	0.64	—	—	—	93.1
525	145	71	69	570	7.3	0.94	—	—	—	87.0
350	135	80	77	775	12.0	0.30	—	—	—	96.4
380	137	—	80	815	9.85	0.106	—	—	—	98.9
450	137	85	82	884	7.8	0.17	—	—	—	97.8
450	137	85	82	924	6.58	0.04	—	—	—	98.4
345	136	89	86	1100	9.96	0.151	11.6	14.2	22.2	97.6
330	130	90	87	1150	9.28	0.155	22.4	7.2	8.1	98.4
400	>150	90	86.5	1280	9.04	0.193	13.8	5.0	7.5	98.0
—	136	84	81	1310	12.0	0.45	31.2	12.5	11.6	96.4
—	139	94	89	1900	11.1	0.093	11.0	13.2	28.3	99.2

Key:
(1) Temperature of smoke °C
(2) System resistance millimeter water column
(3) Dust content in smoke gram K^+/meter^3
(4) Concentration of alkaline solution (percent)
(5) Degree of purification (percent)
(6) Entering smoke
(7) After spray cup
(8) After bubble tower
(9) Exhausted smoke
(10) Entering smoke
(11) Exhausted smoke
(12) Spray cup
(13) Bubble tower
(14) Venturi tube

It is believed that under specified operating conditions, recovery of the ionization additives in smoke--potassium carbonate--by washing with seeded solution using the "spray--bubble--venturi" system in magnetic hydrodynamic power generation can satisfy economic demands and smoke exhaust standards. The recovery rate can reach over 99 percent. The content of potassium carbonate in the exhausted smoke is under 0.2 gram/meter^3.

When using potassium salt additives, the recovered substance contains such salts as potassium carbonate, potassium hydrocarbonate, and potassium sulfate. When using the wet recovery method, three kinds of solutions are obtained, forming a quaternary system of K_2CO_3 - $KHCO_3$ - K_2SO_4 - H_2O. Drawing and using the isotherm solubility diagram of the quaternary system K_2CO_3 - $KHCO_3$ - K_2SO_4 - H_2O have a practical guiding significance for the composition of solutions of the wet recovery method and selection of concentration. The basic requirement is to avoid the production of crystals in the recovery operation. Seen from the phase figure 2, there are two aspects: (1) The proportional relationship among the three salts is at the point of the triangle on the bottom surface. The proportional relationship between potassium hydrocarbonate is mainly determined

Table 2. Table of Data of Retrieval of Additives in Simulated Steam Supply Experiment

(1) 烟气量 HM'/h	温度(2) °C 进气	排烟	阻力降(3) 毫米水柱 系统	文氏管	(4) 碱液循环量 M'/h 喷杯	泡沫塔	文氏管	(5) 烟气含尘克K·/M' 进气	泡沫塔后	(15)(16) 排烟	(6) 净化度 %
2010	370	45	422	2 2	—	6	2	5.08	—	0.365	92.6
2010	360	44	435	266	~20	6.7	2.3	5.55	—	0.33	93.7
2010	380	45	694	432	20	11.3	2.8	4.6	3.29	0.21	95.2
2910	390	40	1275	942	20	10.1	2.1	2.82	1.44	0.025	99.0
2930	460	44	1455	1035	9	10	3	2.04	—	0.04	98.7
2930	330	41	1530	1154	9.3	10.2	3.3	2.64	—	0.017	99.2
3000	300	44	1265	977	20	10.1	2.5	2.33	1.27	0.067	97.2
3080	324	49	1440	970	20	10.8	2.5	2.62	0.855	10.04	98.5
3000	280	54	3290	962	20	10.2	2.6	3.59	0.576	10.04	98.7
3000	340	56	1290	1044	20	—	2.6	2.07	—	0.019	99
3000	320	58	1418	1140	20	—	2.6	2.35	—	0.019	99

Key:

(1) Amount of smoke
(2) Temperature °C
(3) Resistance drop, millimeter of water column
(4) Amount of circulation of alkaline solution M^3/h
(5) Dust content in smoke K^+/M^3
(6) Degree of purification (percent)
(7) Entering steam
(8) Exhausting smoke
(9) System
(10) Venturi tube
(11) Spray cup
(12) Bubble tower
(13) Venturi tube
(14) Entering steam
(15) After bubble tower
(16) Exhausting smoke

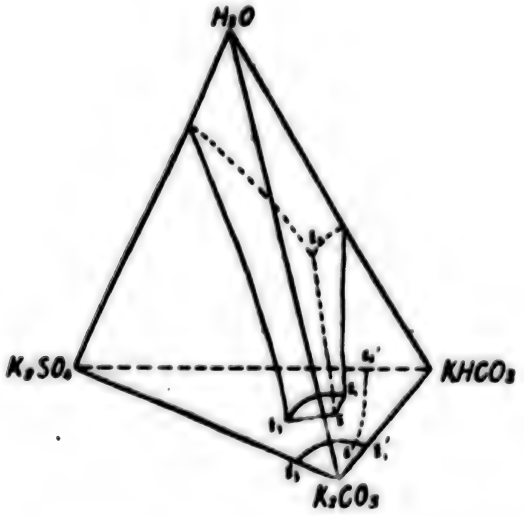

Figure 2. K_2CO_3 - $KHCO_3$ - K_2SO_4 - H_2O
Diagram of isotherm solubility of the quaternary system

by the partial pressure of carbon dioxide in the smoke while the content of potassium sulfate must be selected. If this content is chosen too high, the point of the graph of the solution composed of this dissolved substance will easily touch the surface of the giant crystal of potassium sulfate. If it is chosen too low, the amount of the solution extracted for regeneration operations will increase. (2) The content of water in the solution when the relative contents of the three types of salts are selected is still a free amount. This variable in the phase diagram determines the spatial height of the point of the diagram. If it is chosen too low, it will similarly yield crystals. If it is chosen too high, the content of water will be too large and the amount of heat consumed is recycling and use will increase. The point of the diagram of the solution in recovery operations in principle should approach point E, but must not touch each saturation surface. The actual composition of the solution and concentration should be determined by experiment and with reference to the phase diagram drawn.

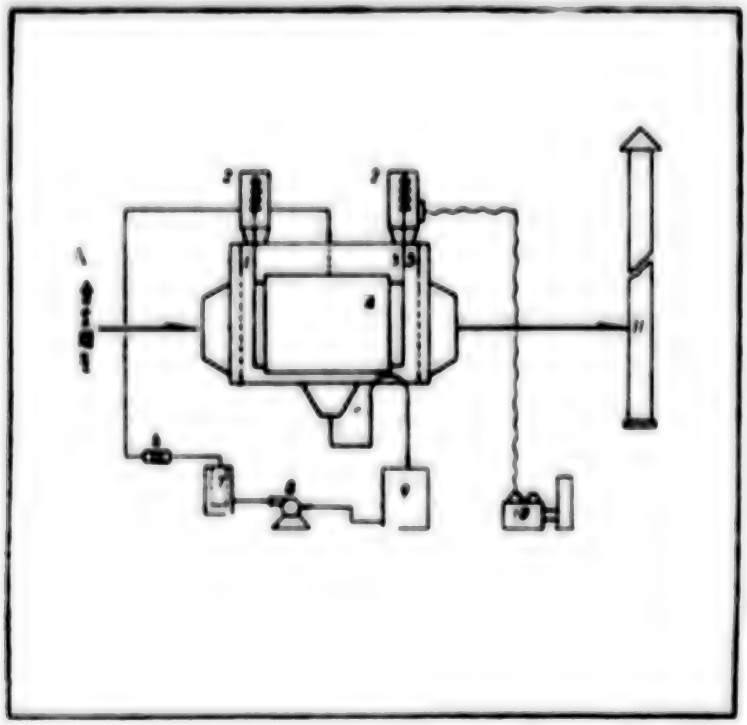

Figure 3. Experimental installation of the wet wall type precipitator

Key: A Dust containing smoke
(1) Gas distribution board
(2) Handling box
(3) Electrical corona frame
(4) Precipitation pole
(5) Static separation board
(6) Flow meter
(7) Filter
(8) Pump
(9) Circulation trough
(10) High voltage rectifier power source
(11) Smoke stack

The flow chart of the wet electrostatic dust precipitator experiment is shown in Figure 3. The reason for using the wet method for recovering dust electrostatically is the consideration that the powdery dust of potassium carbonate is fine and its specific electrical resistance is relatively high (actually measured at 4.7×10^{10} ohms·centimeter), suitable for the conditions of electrostatic recovery of dust. The effective sectional area of a small scale wet electrostatic dust precipitator is 0.64 meters^2. The flat board's precipitation pole is 3 meters long. The distance between the boards is 250 millimeters. There are two sets of atomizing and spraying spout in front of the electrical field. There are also atomizing and spraying spouts or wall-washing spraying tubes lengthwise. In front of the electrical field is an air flow distributing plate. In the back is a double layer electrostatic separation board. A spiked corona wire and a manually operated electron tube rectifier power source are used. The experiment can be conducted jointly with the boiler's experimental support and can also be connected to the power generator group for joint operation. The content of K^+ in the sample solution can be measured by the flame brightness method. Records of the test runs of the wall-washed electrostatic dust precipitator are shown in Table 3. The supply voltage is 47 to 57 KV, when the velocity of air flow is between 0.6 and 0.7 meter/second, the dust recovery efficiency is above 90 percent, reaching a highest of 98 percent. The lowest exit dust content is below 200 milligrams/meter^3, generally between 200 and 500 milligrams/meter^3. When the air flow surpasses 0.7 meter/second, the exit dust content will increase.[7,8]

Table 3. Record of Test Run of the Washed Wall Electrostatic Precipitator

序(1)号	(2)气量 米³/时	(3)气速 米/秒	(4)进气温度 ℃	(5)操作电压 KV	(6)工作电流 mA	(7)火焰光度计测定 进(8)口 K_2CO_3 克/米³	出(9)口 K_2CO_3 克/米³	η %
1	1450	0.64	76	57	7.5	8.55	0.178	97.92
2	1600	0.70	82	57	7.0	9.26	0.285	96.92
3	1700	0.74	83	54	6.0	9.61	0.214	97.77
4	1750	0.76	83	49	5.5	7.09	0.570	92.00
5	1950	0.85	86	51	6.0	7.78	0.570	92.70
6	2050	0.895	86	51	6.0	7.48	0.534	92.84
7	1500	0.65	80	51	5.5	1.64	0.214	87.00
8	1900	0.625	81	57	6.5	9.43	0.570	93.96
9	2100	0.915	84	54	6.0	9.61	0.785	91.86
10	2300	1.00	84	54	6.0	9.61	0.855	91.10
11	1750	0.76	82	53	6.0	9.15	0.570	93.76
12	—	—	—	—	—	9.94	0.570	94.26
13	1800	0.715	83	50	7.5	9.45	0.712	92.62
14	—	—	—	—	—	11.45	0.605	94.68

Key:
(1) Numerical order
(2) Amount of steam meter^3/hour
(3) Velocity of steam meter/second
(4) Temperature of entering steam °C
(5) Operating voltage KV
(6) Operating current mA
(7) Flame brightness meter measurements
(8) At entry K_2CO_3 gram/meter^3
(9) Exit K_2CO_3 gram/meter^3

The structure of the wet electrostatic dust precipitator is simple. Using a small amount of solution can achieve good polar plate washing results. The partial electrostatic plate can help increase the efficiency. The entire polar plate is resistant to erosion and is durable. Further improvement of the structure of the installation (adding a separation plate to prevent shortage, improving the quality of installation of the electrodes and hanging insulation etc) and using automatically controlled power sources will further reduce the concentration of the content of exit dust of the installation.

IV Several Views

The recovery of the ionization additives in magnetic hydrodynamic power generation requires a very high efficiency. The bag type filter, the venturi tube washer and the electrical dust precipitator are three possible high performance dust precipitation installations to be used. The bag type dust eliminator can have a high efficiency but it is bulky. It requires frequent maintenance. Pressure loss is large and it is not used much in industry. The venturi tube washer has outstanding functions. Its structure is simple, operation is stable, building speed is fast, but in operation its resistance loss is still large. The electrostatic dust precipitator exerts direct force upon the suspended bodies, therefore it can operate with low resistance and high efficiency. It has become an ideal dust elimination installation. Theoretically it can collect dust particles of any size. In actual use, when collecting fine powdery dust of high electrical resistance, the efficiency of the dry electrostatic dust precipitator will drop because of such phenomena as the occurrence of reverse electrical corona and dust flying a second time. Although the wet electrostatic dust precipitator can by nature solve these shortcomings of the dry electrostatic dust precipitator, but a large amount of the recovered substance is in a dissolved state.

Worth mentioning is the recent development of the mixed-dry-wet type (hybrid type) electrostatic dust precipitator. It possesses the original advantage of having a low resistance drop of the electrostatic dust precipitator and has also effectively overcome the shortcoming of the wet electrostatic dust precipitator. In such recovery equipment, most of the powdery dust is trapped by the dry part. A small amount of fine powdery dust enters the wet recovery part. Because the phenomena of the occurrence of reverse electrical corona and dust flying a second time have been overcome, even ultrafine particles can be trapped and the concentration of the content of exiting dust can be effectively reduced. The dry powdery dust recovered by the dry part can be directly used as the solid additive seeds (ionization additives) for magnetic-hydrodynamic power generation while a small amount of solution can facilitate regeneration. Therefore, this type of dust recovery equipment has a bright future of being used in magnetic hydrodynamic power generation.

REFERENCES

1. R. J. Rosa (?): Magnetic Hydrostatic Generation, translated by the Scientific Research Group on Magnetic Hydrostatic Generation of Nanjing Engineering Academy, Science Press, 1975

2. V. A. Kirilina and A. E. Sheindlina: MHD Method To Obtain Electrical Energy, ENERGY, 1972.

3. V. A. Starikovey and dr.: A Lengthy Introduction and Conclusion on Ionization Additives on the Y-25 Equipment, TBT, No 2, 1974.

4. J. Haywood and B.J. Womack: Open Cycle MHD Power Generation, London 1969.

5. Methods of Measuring the Concentration of Potassium Containing Aerosol, Material of the Ionization Additives Retrieval Group of the Nanjing Chemical Engineering Research Institute, 1978.

6. Experimental Research in the Method of Wet Retrieval of Ionization Additives, Material of the Ionization Additives Retrieval Group of the Nanjing Chemical Engineering Research Institute, 1976.

7. Report on the Experiment of the Phase Diagram of the K_2CO_3 - $KHCO_3$ - K_2SO_4 - H_2O Quaternary System, Material of the Ionization Additives Retrieval Group of the Nanjing Chemical Engineering Research Institute, 1977.

8. Guhe Mining Company's Electrical Dust Collector, Material of the Nanchang Nonferrous Metallurgy Design Academy, 1976.

9. Ito Hiro (?), Saidogu, Ikami Kenjiro: Measurements in Separating Powder and Dust and the Process of Collecting Dust on Top in the Cement Industry, JIZHUANG, Vol 16, No 8, 1977.

9296
CSO: 8111/0226

BALANCING FLEXIBLE SHAFT GYRO ROTOR STUDIED

Nanjing NANJING GONGXUEYUAN XUEBAO [JOURNAL OF NANJING INSTITUTE OF TECHNOLOGY] in Chinese No 4, Dec 79 pp 72-85

[Article by Cha Liguan [2686 4409 0385]: "The Gyroscope Vibration Research Group of the Research Laboratory of Gyroscope Principles and Application." This article was received in April 1979. Second draft completed on 25 August]

[Text] The Problem of Balancing the Flexible Shaft Gyro Rotor

Abstract

In the past 10 years, many methods for balancing the flexible shaft rotor have been proposed and used. These methods can be classified into two types, depending on whether the shaft is balanced as a rigid body. This article centers on the factors that affect the sensitivity of balance of the flexible shaft rotor. In addition, the article also suggests some ways to improve the dynamic balance of the flexible shaft gyro rotor.

I. Introduction

The gyro motor is the key element that affects the precision and life of the gyroscopic instruments. In stabilization equipment, aviation, navigation, guided missiles and man-made satellites, the gyroscopic inertia and precession of the gyroscope can be used to make various types of gyro equipment such as the azimuth compass, altazimuth, azimuth level, gyrocompass, stabilizer platform, autopilot and guidance systems. But the characteristics of the gyroscope are only manifested when the rotor rotates at high speeds and the faster the rotation the more pronounced the characteristics of the gyroscope. Therefore, the speed of rotation of ordinary gyro rotors is all above 20,000 revolutions/minute, some can rotate at 100,000 revolutions/minute. Because the rotary axis of the rotor shifts to the axis of inertia, a dynamic imbalance is produced leading to the occurrence of inertia and inertial moment, and the gyroscope drifts. For example, a gyro rotor weighing one kilogram and whose longitudinal shift of the center of gravity of the rotor is e = 0.002 millimeter will have an inertia F of:

$$F = \frac{G}{g} e \left(\frac{\pi n}{30}\right)^2 = \frac{1}{9.8} \times 0.002 \times 10^{-3} \times \left(\frac{\pi \times 24 \times 10^3}{30}\right)^2 = 1.29 \text{ kg}$$

The dynamic imbalance of the high speed rotor will cause the entire gyro to vibrate and will add a dynamic load, causing the gyro to undergo additional drift on the one hand and affect the precision of the gyroscope, and on the other hand, the life of the gyroscope is also affected. Improving the balance of the gyroscope serves importantly to improve the precision of the gyroscope and prolong the life of the gyroscope. At present, some factories in our nation that manufacture gyroscopes use machine balancing techniques to balance them. Some abnormal phenomena have occurred in the process of balancing when using these balancing techniques. For example, when balancing on the balancing machine, the stationary imbalance or dynamic imbalance of the rotor in the vibration system cannot be shown. Sometimes a rotor which has been balanced as required on the balancing machine manifests imbalance when the balancing speed of rotation or the bearing rigidity is changed. These problems were discussed at the Second National Academic Conference on Dynamic Balance held in Fuzhou. It was believed that theoretical analysis of the balance of rotors is necessary for finding some effective methods to improve the precision of dynamic balance of rotors. This article discusses some preliminary analysis of the balancing of flexible shaft gyro rotors.

II. Vibration Model of Dynamic Balance of the Gyro Rotor

The causes of imbalance of the gyro rotor are many, such as improper structural design of the gyro rotor, the effects of magnetic moment of the hysteresis motor, unequal elasticity of the materials, improper matching of materials with different thermal expansion coefficients, effects of damping in air, will all affect the balance of the rotor. Let us take the dynamic balance of the elastic thin walled flexible shaft rotor of the navigational compass (model 601) to study the vibration model in the process of dynamic balancing of the flexible shaft rotor. Figure 1 shows the vibration model of the flexible shaft rotor on the dynamic balancing machine. The rotor and the shaft housing form a rotary system supported on the elastic support of the dynamic balancing machine. When the rotor is stationary on the elastic support of the balancing machine, the center of mass of the rotor 0' coincides with the origin 0 of the fixed coordinates system $O\xi\eta\zeta$. The $O\eta$ axis and the axial line of the stationary gyro rotor are consistent. The positive direction and the direction of the vector of the angular velocity of the gyro rotor are consistent. When the axis of the gyro rotor undergoes flexible deformation, the center of mass of the rotor system is at 0'. The coordinates xyz of 0' and the gyro are connected but they do not participate in the spinning movement of the gyro rotor. The direction of the coordinate axis 0'x and the direction of the tangent line at the center of the mass of the rotary shaft are consistent. The origin 0' of the coordinate system is determined by the position of the center of mass of the rotor when axis of the rotor undergoes flexible deformation. When the gyro rotor rotates at angular velocity ω, a forced vibration of the rotor system is caused by the unbalanced inertia due to the imbalance of the quality of the rotor. To study the relationship between the rotary angles of the dynamic coordinates system 0'xyz and the fixed coordinates system $O\xi\eta\zeta$, we first allow the origin 0' of the dynamic coordinates system to coincide with the origin of the fixed coordinates system as shown in Figure 2. The angle α is the rotary angle about the $O\zeta$ axis of the dynamic coordinates 0'xyz and β is the rotary angle about the Oz axis of the dynamic coordinates 0'xyz. The positive directions of the vectors i, $\dot{\beta}$, and ω of the angular velocity are determined by the right hand spiral method. The positive directions of $\dot{\alpha}$, $\dot{\beta}$, and ω are in the

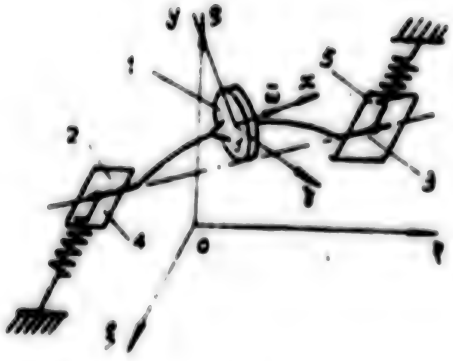

Figure 1. Simple diagram of the gyro rotor of or the 601 model compass

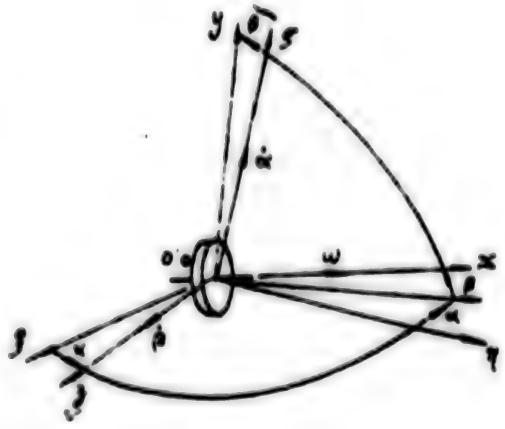

Figure 2. The relationship between the coordinates system O'xyz and Oξηζ

positive directions of the ζ, z and x axis respectively. When the center O' of mass of the rotor moves relative to the origin O of the fixed coordinates system, the position of the point O' can be determined from the coordinates of O' of the fixed coordinates system Oξηζ. When the system undergoes deformation in the vibration process, its spatial position is determined by the coordinates ξ, η, ζ and α, β which determine the spatial position of the point O'.

III. The Equation of Motion of the Gyro Rotor

To write down the systematic equations of motion, we can analyze the motion in the O horizontal surface and the O vertical surface. First we find the dynamic energy and potential energy of the system. Then we use Lagrange's equations of the second kind to set up the equations of motion for the small vibrations of the system. First we use the projections of $\dot{\alpha}$, $\dot{\beta}$ and ω to calculate the projected values Ωx, Ωy and Ωz of the angular velocity of the rotor on the x,y z axis.

$$\left.\begin{aligned} \Omega_x &= \omega + \dot{\alpha}\sin\beta \\ \Omega_y &= \dot{\alpha}\cos\beta \\ \Omega_z &= \dot{\beta} \end{aligned}\right\} \qquad (1)$$

Angle β is very small and we can regard sin β ≈ β, cos β ≈ 1. The angle θ is the rotary angle of the axial line of the motor housing and the shaft covering components about the vertical axis on the horizontal surface. The angle θ and the angle α are in the same direction. The motor housing and the shaft covering components can be viewed as elements that do not undergo elastic deformation. The difference between α and θ is very small. Because the elasticity of the vibration support is far greater than the elasticity of the shaft of the rotor, this high value small difference can be neglected, i.e., α ≈ θ.

Equation (1) can be written as:

$$\left.\begin{aligned} \Omega_1 &= \omega + \dot{\theta}\beta \\ \Omega_2 &= \dot{\theta} \\ \Omega_3 &= \dot{\beta} \end{aligned}\right\} \qquad (2)$$

Now let us analyze and study the balancing of the gyro motor of the 601 model compass on the A-21 model dynamic balancing machine. If the degree of freedom of the housing components along the axial direction of the rotor is not counted (because the axial rigidity of the rotor is far greater than the horizontal rigidity of the spring), the motor housing and the shaft covering components have two dimensions of freedom of movement in space. The corresponding general coordinates are θ and ξ. Let us set up the equations of motion of small vibrations of the system in the following.

1. Dynamic energy of the system

(1) Dynamic energy of the gyro rotor: The dynamic energy of the gyro rotor consists of horizontal kinetic energy T_1 of the center of mass of the gyro rotor and the rotary kinetic energy T_2 of the center of mass of the gyro rotor.

$$T_1 = \frac{1}{2} M_1 \quad (\dot{\xi}^2 + \dot{\zeta}^2)$$

M is the mass of the gyro rotor.

$\dot{\xi}$, $\dot{\zeta}$ are the projections of the velocity of the center of mass of the gyro rotor on the ξ and ζ axis.

$$T_2 = \frac{1}{2} I_0 \Omega_1^2 + \frac{1}{2} I (\Omega_2^2 + \Omega_3^2)$$

$$= \frac{1}{2} I_0 \omega^2 + I_0 \omega \dot{\theta}\beta + \frac{1}{2} I (\dot{\theta}^2 + \dot{\beta}^2)$$

I_0, I are respectively the inertia of the polar rotation of the gyro rotor and the inertia of the equatorial rotation.

(2) The kinetic energy T_3 of the gyro motor housing and the housing components: The spatial position of the gyro motor housing and the housing components is determined by the general coordinates ξ and ζ. Their movement consists of horizontal movement in the ξ direction and the rotation about the vertical axis (θ is the angle of rotation).

$$T_3 = \frac{1}{2} M_3 \dot{\xi}^2 + \frac{1}{2} I_3 \dot{\theta}^2$$

M_2, I_2 are respectively the mass of the gyro motor housing and the housing components and the equatorial inertia.

(3) Kinetic energy T_4 of the vibrating supports: First we find the velocities of horizontal movements of the two left and right vibrating supports $\dot{\xi}_{left}$ and $\dot{\xi}_{right}$.

$$\dot{\xi}_{left} = \dot{\xi} + \dot{\theta} l_{left} \qquad \dot{\xi}_{right} = \dot{\xi} - \dot{\theta} l_{right}$$

l_{left} and l_{right} respectively represent the distances between the center of mass of the rotor and the left and right vibrating supports

$$T_4 = \frac{1}{2} M_3 (\dot{\xi} + \dot{\theta} l_{left})^2 + \frac{1}{2} M_3 (\dot{\xi} - \dot{\theta} l_{right})^2$$

$$= M_3 \dot{\xi}^2 + M_3 \dot{\theta} \dot{\xi} (l_{left} - l_{right}) + \frac{1}{2} M_3 \dot{\theta}^2 (l_{left}^2 + l_{right}^2)$$

M_3 is the mass of each vibrating support.

The total kinetic energy T of the system is:

$$\begin{aligned} T &= T_1 + T_2 + T_3 + T_4 \\ &= \frac{1}{2} M_1 (\dot{\xi}^2 + \dot{\zeta}^2) + \frac{1}{2} I_1 \omega^2 + I_1 \omega \dot{\theta} \beta \\ &\quad + \frac{1}{2} I (\dot{\theta}^2 + \dot{\beta}^2) + \frac{1}{2} M_2 \dot{\xi}^2 + \frac{1}{2} I_2 \dot{\theta}^2 + M_3 \dot{\xi}^2 \\ &\quad + M_3 \dot{\theta} \dot{\xi} (l_{\pm} - l_{\mp}) + \frac{1}{2} M_3 \dot{\theta}^2 (l_{\pm}^2 + l_{\mp}^2) \end{aligned} \tag{3}$$

2. Potential energy of the system in spatial motion

When the system is in spatial motion, the shaft of the gyro rotor is subject to the inertia P_ζ and the inertia moment M_ξ (as shown in Figure 3). The elastic deformation on the horizontal surface is very small and can be neglected. Thus, the potential energy Π of the system consists of the potential energy Π_1 of the elastic force of the restoration of the spring of the vibrating support, the potential energy $\Pi_{P\zeta}$ of the system caused by the inertia P_ζ on the rotor and potential energy $\Pi_{M\xi}$ of the system caused by the inertia moment M_ξ on the rotor.

(1) Potential energy Π_1 of the force of restoration of the spring of the vibrating support.

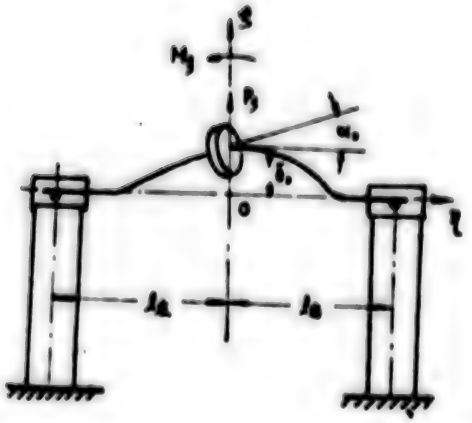

Figure 3. Illustration of the positional shift of the rotor's axis under the inertia and the inertia moment forces

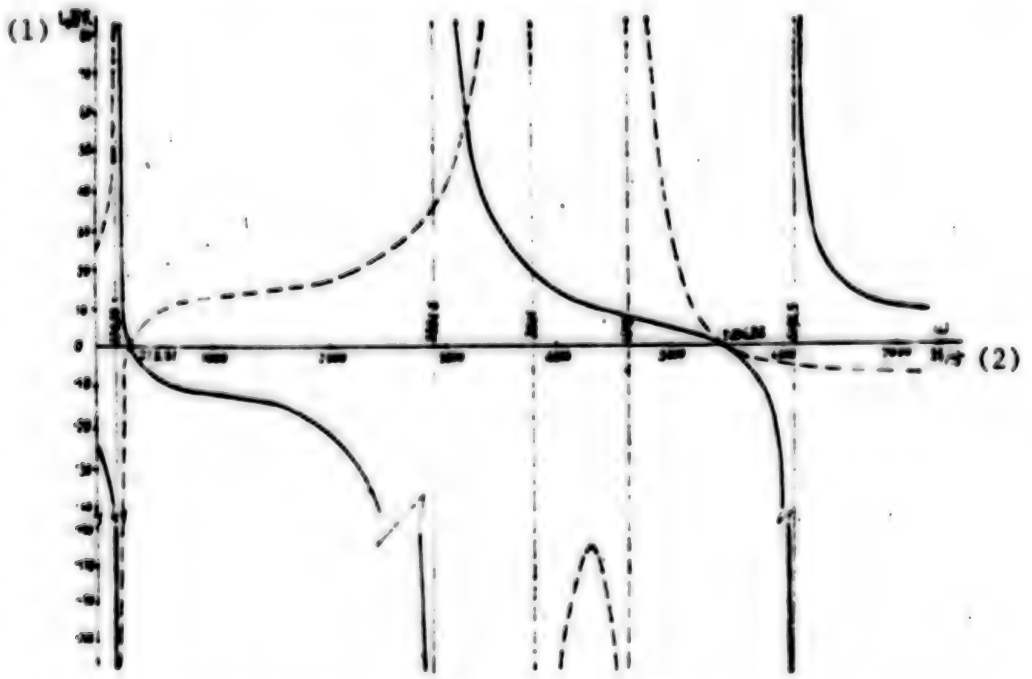

Figure 4. Relationship between the balanced speed of rotation and the vibration center distance Lv

Key: (1) centimeter
(2) revolutions/minute

solid line -- the unbalanced amount is in the right balance plane
dotted line-- the unbalanced amount is in the left balance plane

$$\Pi_1 = \frac{1}{2} k (\xi + \theta l_{left})^2 + \frac{1}{2} k (\xi - \theta l_{right})^2$$
$$= k\xi^2 + k\xi\theta (l_{left} - l_{right}) + \frac{1}{2} k\theta^2 (l_{left}^2 + l_{right}^2) \quad (4)$$

k is the elastic coefficient of the spring.

(2) The elastic change in position δ_0 and the rotary angle α_0 caused by the effects of the inertia moment M_ξ and the inertia P_ζ on the axis of the rotor under elastic deformation potential energy $\Pi_{P\zeta}$ and $\Pi_{M\xi}$ of the axis of the gyro rotor can be determined by the following equations:

$$\left.\begin{aligned} \delta_0 &= a_{11} P_i + a_{12} M_i \\ \alpha_0 &= a_{21} P_i + a_{22} M_i \end{aligned}\right\} \quad (5)$$

where α_{11}, α_{12} represent the changes in position of the axis of the rotor from the location of the center of mass of the rotor caused respectively by the unit force and the unit moment at the center of mass of the gyro rotor, and α_{21}, α_{22} represent the rotary angles at the center of mass of the gyro rotor caused by the respective unit force and unit moment on the axis of the rotor.

Figure 5 shows the changes in position at the center of mass of the gyro rotor under the effects of inertia P_ζ and inertia moment M_ξ. The relationship between α_{11}, α_{12}, α_{21}, α_{22} and inertia P_ζ and inertia moment M_ξ can be solved.

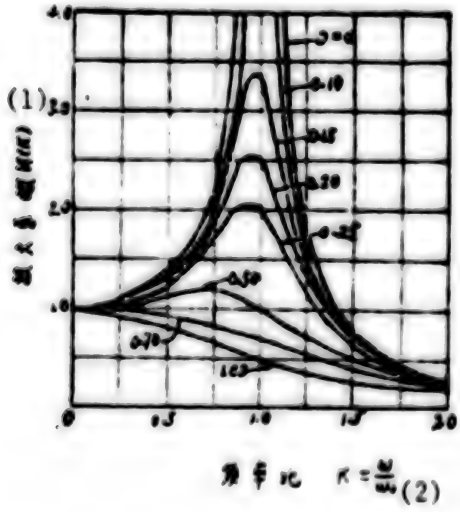

Figure 5. Characteristic curve of amplitude and frequency

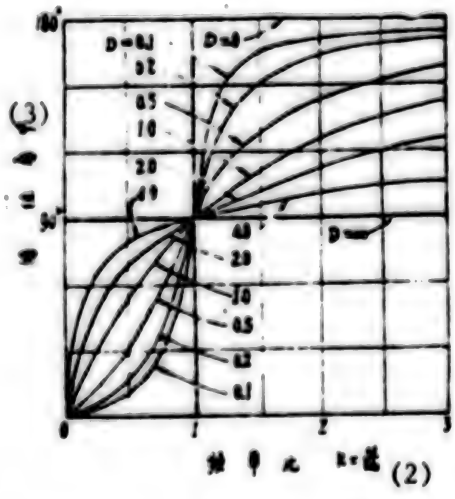

Figure 6. Characteristic curve of phase and frequency

Key:
(1) Magnificent coefficient
(2) Frequency ratio
(3) Phase angle φ

Solving equation (5) we have:

$$P_i = -\frac{a_{12}}{a_{11}a_{22}-a_{21}a_{12}}\delta_0 - \frac{a_{11}}{a_{11}a_{22}-a_{21}a_{12}}a_0 = C_{11}\delta_0 - C_{12}a_0$$

$$M_i = -\frac{a_{21}}{a_{11}a_{22}-a_{21}a_{12}}a_0 - \frac{a_{21}}{a_{11}a_{22}-a_{21}a_{12}}\delta_0 = C_{21}a_0 - C_{22}\delta_0 \qquad (6)$$

$$C_{11} = \frac{a_{22}}{a_{11}a_{22}-a_{21}a_{12}} \qquad C_{12} = \frac{a_{12}}{a_{11}a_{22}-a_{21}a_{12}}$$

$$C_{21} = \frac{a_{21}}{a_{11}a_{22}-a_{21}a_{12}} \qquad C_{22} = \frac{a_{11}}{a_{11}a_{22}-a_{21}a_{12}}$$

By the commutative law, $\alpha_{12} = \alpha_{21}$, thus $C_{12} = C_{21}$. Also, we know from Figure 2 and Figure 3, $\alpha_0 \approx P$, $\delta_0 \approx \zeta_0$. Thus the deformation potential energy $\Pi_{P\zeta}$ and $\Pi_{M\xi}$ under the inertia P_ζ and inertia moment M_ξ can be calculated:

$$\Pi_{Pi} = \frac{1}{2} P\zeta \cdot \zeta = \frac{1}{2} C_{11}\zeta^2 - \frac{1}{2} C_{12}\zeta\beta$$

$$\Pi_{Mi} = \frac{1}{2} M_i \cdot \beta = \frac{1}{2} C_{22}\beta^2 - \frac{1}{2} C_{12}\zeta\beta$$

The potential energy of the entire system is:

$$\Pi = \Pi_1 + \Pi_{Pi} + \Pi_{Mi} = k\xi^2 + k\xi\theta(l_{left} - l_{right}) + \frac{1}{2} k\theta^2 (l_{left}^2 + l_{right}^2) + \frac{1}{2} C_{11}\zeta^2 + \frac{1}{2} C_{22}\beta^2 - C_{12}\beta\zeta \qquad (7)$$

The unbalanced mass of the rotating part of the gyro motor is m_1, the radial distance r is deviation of the axial line from the center of mass of the rotor, when the gyro rotor rotates at an angular velocity of ω, the centrifugal inertia acting upon the center of mass of the rotor is $F_{LL} = m_1 r\omega^2$.

Simplifying this force to the origin of the coordinates yields two forces and two double moments of force as follows:

$$F_\zeta = m_1 r\omega^2 \cos(\omega t + \varphi)$$

$$F_\xi = m_1 r\omega^2 \sin(\omega t + \varphi)$$

$$M_\zeta = m_1 r\omega^2 h \sin(\omega t + \varphi)$$

$$M_\xi = m_1 r\omega^2 h \cos(\omega t + \varphi)$$

F_ζ, F_ξ are the forces acting along the ζ or ξ axial direction at the origin of the coordinates.

M_ζ, M_ξ are the moments about the ζ or ξ axis, h is the distance of deviation along the ξ axis of the center of mass of the gyro rotor.

Now we apply the Lagrangian equation

$$\frac{d}{dt}\left(\frac{\partial L}{\partial \dot{q}_i}\right) - \frac{\partial L}{\partial q_i} = Q_i$$

$$L = T - \Pi \qquad i = 1, 2 \cdots\cdots$$

and substitute the values into the above equation, we obtain the group of differential equations of forced vibration:

$$\left.\begin{aligned}
&(M_1 + M_2 + 2M_3)\ddot{\xi} + 2k\xi + M_3\ddot{\theta}(l_{左}^{*} - l_{右}^{**}) + k\theta(l_{左}^{*} - l_{右}^{**}) \\
&\quad = m_1 r\omega^2 \sin(\omega t + \varphi_1) \\
&M_1\ddot{\zeta} + C_{11}\zeta - C_{12}\beta = m_1 r\omega^2 \cos(\omega t + \varphi_1) \\
&[I + I_2 + M_3(l_{左}^{*2} + l_{右}^{**2})]\ddot{\theta} + I_0\omega\dot{\beta} + k\theta(l_{左}^{*2} + l_{右}^{**2}) \\
&\quad + M_3\ddot{\xi}(l_{左}^{*} - l_{右}^{**}) + k\xi(l_{左}^{*} - l_{右}^{**}) = -m_1 r\omega^2 \sin(\omega t + \varphi_1) \\
&I\ddot{\beta} - I_0\omega\dot{\theta} - C_{21}\zeta + C_{22}\beta = m_1 r\omega^2 h \cos(\omega t + \varphi_1)
\end{aligned}\right\} \qquad (8)$$

[* = left ** = right]

On the dynamic balancing machine, $l_{left} = l_{right} = 1$. The above equations are simplified to:

$$\left.\begin{aligned}
&(M_1 + M_2 + 2M_3)\ddot{\xi} + 2k\xi = m_1 r\omega^2 \sin(\omega t + \varphi_1) \\
&M_1\ddot{\zeta} + C_{11}\zeta - C_{12}\beta = m_1 r\omega^2 \cos(\omega t + \varphi_1) \\
&(I + I_2 + 2M_3 l^2)\ddot{\theta} + I_0\omega\dot{\beta} + 2kl^2\theta = -m_1 r\omega^2 h \sin(\omega t + \varphi_1) \\
&I\ddot{\beta} - I_0\omega\dot{\beta} - C_{21}\zeta + C_{22}\beta = m_1 r\omega^2 h \cos(\omega t + \varphi_1)
\end{aligned}\right\} \qquad (9)$$

IV. Center of Vibration and Distance of the Center of Vibration

When the gyro rotor is balanced on the balancing machine, its equations of motion are as shown in equations (9). The terms ξ and ζ are the shifts of horizontal movement and θ and β are the angular shifts of rotary motion, ω is the speed of rotation of the gyro rotor during the process of balancing and is the balanced rotary speed. The entire rotor system--including the gyro rotor, motor housing, housing components--is supported on the vibration measuring support. The support transmits the small vibrations to the transducer and the transducer transmits the signals to the display equipment.

Now we solve equations (9). Let the special solution of equations (9) be:

$$\left.\begin{aligned} \xi &= a_1 \sin(\omega t + \varphi_1) \qquad \zeta = a_2 \cos(\omega t + \varphi_1) \\ \theta &= a_3 \sin(\omega t + \varphi_1) \qquad \beta = a_4 \cos(\omega t + \varphi_1) \end{aligned}\right\} \tag{10}$$

Differentiating equations (10) and substituting the results of differentiation and equations (19) simultaneously into equations (9) and after arranging the terms we obtain the following equations:

$$\left.\begin{aligned} &[2k - (M_1 + M_2 + 2M_3)\omega^2]a_1 = m_1 r\omega^2 \\ &(C_{11} - M_1\omega^2)a_2 - C_{12}a_4 = m_1 r\omega^2 \\ &[2kl^2 - (I + I_2 + 2M_3 l^2)\omega^2]a_3 - I_0\omega^2 a_4 = -m_1 r\omega^2 h \\ &(C_{12} - I\omega^2)a_4 - I_0\omega^2 a_3 - C_{12}a_2 = m_1 r\omega^2 h \end{aligned}\right\} \tag{11}$$

From equations (11) we can solve a_1 and a_3:

$$\left.\begin{aligned} a_1 &= \frac{m_1 r\omega^2}{2k - (M_1 + M_2 + 2M_3)\omega^2} \\ a_3 &= \frac{\Delta_\theta}{\Delta} m_1 r\omega^2 \end{aligned}\right\} \tag{12}$$

where

$$\Delta = \begin{vmatrix} C_{11} - M_1\omega^2 & 0 & -C_{12} \\ 0 & 2kl^2 - (I + I_2 + 2M_3 l^2)\omega^2 & -I_0\omega^2 \\ -C_{12} & -I_0\omega^2 & C_{12} - I\omega^2 \end{vmatrix}$$

$$\Delta\theta = \begin{vmatrix} C_{11} - M_1\omega^2 & 1 & -C_{12} \\ 0 & -h & -I_0\omega^2 \\ -C_{12} & h & C_{12} - I\omega^2 \end{vmatrix}$$

The movement of the axial line of the motor and the housing group is composed of the two parts of horizontal movement and rotary movement. The movement of the entire gyro rotor, motor housing and housing group is about a certain point. Such a point is called the system's vibration center. The distance from the center of mass of the gyro rotor to the vibration center can be called the vibration center distance, designated L_v.

$$Lv = \frac{\xi}{\theta} = \frac{a1}{a_3} = \frac{\Delta}{[2k - (M_1 + M_2 + 2M_3)\ \omega^2]\ \Delta_\theta} \tag{13}$$

V. Static Loss of Vibration and Dynamic Loss of Vibration

The periodic movement of the left and right supports of the balancing machine is related to the vibration center distance L_v. Now we discuss two special situations:

1. $L_v \to \infty$

When $\Delta \neq 0$, but $2k-(M_1+M_2+2M_3)\omega^2=0$ 时, $L_v \to \infty$。

At this time, the value of angular shift shows the angular vibration component is $\theta = \frac{\xi}{L_v} = 0$。. This means that regardless of whether a dynamic movement that causes the gyro to undergo angular vibration exists on the gyro rotor, no values of angular shift are shown on the balancing machine. The two vibration supports vibrate at the same amplitude and in the same phase. This is the same as the situation of stationary imbalance. When $L_v \to \infty$ the angular vibration component of the system disappears. Even when there is a dynamic imbalance on the gyro rotor, the balancing machine cannot measure the value of imbalance at this time. We call this phenomenon a dynamic loss of vibration. We know from equations (13) that when $\Delta = 0$:

$$\Delta_\theta = 0 \text{ or}$$

We call the balanced rotary speed ω at this time the rotary velocity of dynamic loss of vibration or rotary velocity of linear vibration. The ω linear vibration can be computed as follows:

When $$2k-(M_1+M_2+2M_3)\omega_{c1}^2=0$$

$$\omega_{c1}^2 = \frac{2k}{M_1+M_2+2M_3} \tag{14}$$

When $\Delta_\theta = 0$

$$-hM_1(I+I_0)\omega_{c2}^4+(I_0C_{11}+h^2C_{11}(I+I_0)+C_{11}M_1])\omega_{c2}^2$$
$$+h(C_{12}^2-C_{11}C_{11})=0 \tag{15}$$

2. $L_v = 0$

When $\Delta_\theta \neq 0$, $\Delta = 0$, $L_v = 0$. We know from equations (10) and equations (13) that when $\Delta = 0$, $a_1 = 0$, $\xi = 0$. The left and right vibrating supports of the balancing machine undergo angular vibrations of equal amplitudes and reverse phases. The horizontal vibration component has disappeared. This is the same as the situation when only dynamic imbalance exists. Regardless of whether stationary imbalance exists on the gyro rotor, when $L_v = 0$, the balancing machine cannot measure the value of static imbalance. We call this phenomenon static loss of vibration. The balanced speed of rotation equivalent to the element can be called the rotary velocity of angular vibration or the rotary velocity of static loss of vibration. These rotary velocities can be calculated as follows:

$$
\begin{aligned}
&\Delta_\theta \neq 0,\ \Delta = 0 \\
&(C_{11} - M_1\omega^2)[2hl^2 - (I + I_1 + 2M_1l^2)\omega^2](C_{22} - I\omega^2) \\
&- C_{12}^2[2hl^2 - (I + I_1 + 2M_1l^2)\omega^2] - (I_\theta\omega^2)^2(C_{11} - M_1\omega^2) = 0 \\
&[M_1I_\theta^2 - M_1I(I + I_1 + 2M_1l^2)]\omega^6 + [2hl^2IM_1 + (C_{22}M_1 + C_{11}I) \\
&(I + I_1 + 2M_1l^2) - C_{11}I_\theta^2]\omega^4 + [C_{12}^2(I + I_1 + 2M_1l^2) \\
&- 2hl^2(M_1C_{22} + IC_{11}) - C_{11}C_{22}(I + I_1 + 2M_1l^2)]\omega^2 \\
&+ 2hl^2(C_{11}C_{22} - C_{12}^2) = 0 \qquad (16)
\end{aligned}
$$

In summary, when the gyro rotor is balanced on the dynamic balancing machine, motion of the vibrating system is composed of horizontal movement and rotary motion. The numerical values of the shift ξ of horizontal movement and angular shift θ of rotation vary according to the vibration center distance L_v of the system. When the value of the vibration center distance L_v approaches infinity, the system's angular shift $\theta = 0$. Thus, the phenomenon of dynamic loss of vibration in which only the shift of horizontal movement can be measured and angular shift cannot be measured exists. The corresponding balanced speed of rotation is called the rotary velocity of linear vibration. When the vibration center distance $L_v = 0$, the shift of horizontal movement of the system $\xi = 0$. Thus the phenomenon of static loss of vibration in which only the dynamic imbalance can be measured but the component of stationary imbalance cannot be measured exists. The corresponding balanced speed of rotation is called the rotary velocity of static loss of vibration or the rotary velocity of angular vibration.

VI. Actual Example of Computation

Now we take the thin walled flexible shaft rotor of the 601 model navigational gyro compass as an example to perform numerical calculations.

1. Known parameters

$$I_p = 54\times10^{-3}\ \text{kg cm sec}^2$$
$$I = 28\times10^{-3}\ \text{kg cm sec}^2$$
$$I_p = 13\times10^{-3}\ \text{kg cm sec}^2$$
$$M_1 = 2.25\times10^{-3}\ \text{kg cm}^{-1}\ \text{sec}^2$$
$$M_2 = 0.6990\times10^{-3}\ \text{kg cm}^{-1}\ \text{sec}^2$$
$$M_3 = 0.1653\times10^{-3}\ \text{kg cm}^{-1}\ \text{sec}^2$$

2. Influencing coefficients: C_{11}, C_{21}, C_{12} and C_{22}

The shaft of the gyro rotor of the 601 model is spindle shaped. It is a rotary shaft with a variable section. When computing the influencing coefficients of the rotary shaft we can simplify it and consider it as a stepped shaft. The numerical values computed are:

$$a_{11} = 13.50\times10^{-4}$$
$$a_{12} = a_{21} = 0.4151\times10^{-4}$$
$$a_{22} = 1.087\times10^{-4}$$

According to equations (6), we can compute and obtain:

$$C_{11} = \frac{a_{22}}{a_{11}a_{22} - a_{12}a_{21}} = 750.1$$

$$C_{12} = -\frac{a_{12}}{a_{11}a_{22} - a_{12}a_{21}} = 286.4$$

$$C_{22} = \frac{a_{11}}{a_{11}a_{22} - a_{12}a_{21}} = 93.15$$

3. The frequency of harmonic oscillation of the system

From equations (10):

$$\begin{cases} \xi = a_1 \sin(\omega t + \varphi_1) \\ \theta = a_2 \sin(\omega t + \varphi_2) \end{cases}$$

From equations (12)

when
$$\begin{cases} a_1 = \dfrac{m_1 r\omega^2}{2k - (M_1 + M_2 + 2M_3)\omega^2} \\ a_2 = \dfrac{\Delta_1}{\Delta} m_1 r\omega^2 \end{cases}$$

$2k - (M_1 + M_2 + 2M_3)\omega^2 = 0$ 时, $a_1 \to \infty$, $\xi \to \infty$

$\Delta = 0$ 时, $a_2 \to \infty$, $\theta \to \infty$

Actually, because of the effect of damping, ζ and θ cannot approach infinity but can cause harmonic oscillation.

Now let us find the frequency of linear vibration and the frequency of angular vibration.

ω^2 linear vibration $= -\omega_n = -\frac{2k}{M_1 + M_2 + 2M_3} = 0.3354 \times 10^3$

ω linear vibration = 18.31 radians/second = 174.88 revolutions/minute.

The vibration frequency occurs when $\Delta = 0$. From equations (16) we can obtain the frequency of angular vibration. First we simplify equations (16) as follows:

$$A_4\omega^4 + A_3\omega^3 + A_2\omega^2 + A_1 = 0$$

$$A_4 = M_1 I_3^2 - M_1 I (I + I_3 + 2M_3 l^2)$$

$$A_3 = 2kl^2 I M_1 + (C_{11} M_1 + C_{11} I)(I + I_3 + 2M_3 l^2) - C_{11} I_3^2$$

$$A_2 = -[2kl^2 (C_{11} M_1 + C_{11} I) + (C_{11} C_{11} - C_{12}^2)(I + I_3 + 2M_3 l^2)]$$

$$A_1 = 2kl^2 (C_{11} C_{11} - C_{12}^2)$$

Substituting the values of known parameters for the terms A_0, A_1,..... we have:

$$A_4 = 3.125 \times 10^{-4}$$

$$A_3 = 0.104$$

$$A_2 = -3.785 \times 10^3$$

$$A_1 = 3.111 \times 10^6$$

$$3.125 \times 10^{-4}\omega^4 + 0.104\omega^3 - 3.785 \times 10^3\omega^2 + 3.111 \times 10^6 = 0$$

Solving the above equation we obtain the frequency of harmonic oscillation of vibration:

ω angular vibration 1 = 28.673 radians/second = 273.81 revolutions/minute.

ω angular vibration 2 = 575.63 radians/second = 5496.86 revolutions/minute.

Now we find the rotary velocity of static loss of vibration and the rotary velocity of dynamic loss of vibration:

Rotary velocity of static loss of vibration: The rotary velocity of static loss of vibration is the frequency of angular vibration:

ω_1 = 273.81 revolutions/minute, ω_2 = 5496.86 revolutions/minute.

The rotary velocity of dynamic loss of vibration can be obtained from equations (14) and (15):

When h = 1.6 cm

ω_1 = 174.88 revolutions/minute
ω_2 = 2894.6 revolutions/minute
ω_3 = 6095 revolutions/minute

When h = -1.6 cm

ω_1' = 174.88 revolutions/minute
ω_2' = 3801 revolutions/minute
ω_3' = 4640.1 revolutions/minute

VII. The Vibration Center Distance Curve and Rational Balancing Speed of Rotation

When the flexible shaft rotor is being balanced on the dynamic balancing machine, the curve of variation between the system's vibration center distance L_y and the balancing speed of rotation ω is much more complex than the situation when the shaft rotor is rigid. Table 1 lists the relationship between the vibration center distance L_y and the balancing speed of rotation when the gyro rotor of the 601 model compass is being balanced on the A-21 model dynamic balancing machine. Figure 4 shows the curve drawn from the points of functional relations between the two. The solid line h is the curve of positive values. The dotted line h is the curve of negative values. Figure 4 shows that the solid line and the dotted line are symmetric about the horizontal axis in some regions while in other regions they are basically symmetric and in some other regions they are asymmetrical. In the regions where the solid line and the dotted line are symmetrical about the horizontal axis, as long as the center of mass of the rotor is at the midpoint of the two left and right supports, the balancing speed of rotation is relatively far away from the frequency of loss of vibration. Under this situation, the center distances L_y of the vibrating system are equal but in opposite direction. When an unbalanced weight exists on the right balance plane and the right transducer shows a certain value ε, and when the same unbalanced weight exists on the left balance plane, the value shown by the left transducer is equivalent to ε and corresponds to it. This conforms to the demands of the test. But in certain regions in Figure 4, the solid line and the dotted line are on the same side of the horizontal axis. At this time, regardless of whether the unbalanced weight is on the left balance plane or the right balance plane, the direction of this imbalance shown by the left (or right) transducer will be the same. This means, the measuring system of the balancing machine cannot differentiate the signal of

Table 1. Relationship Between the Balancing Speed of Rotation ω and the Vibration Center Distance L_v

ω	(1) 转/分	0	100	150	174.88	200	273.81	500	1000	1500	2000	2500
	(2) 弧度/秒	0	10.5	15.7	18.313	20.9	28.673	52.4	105	157	209	262
L_v	(3) 实线(厘米)	25.6	33.1	−67.8	±∞	37.9	−0.000	−8.6	−11.6	−14.7	−21.4	−46.4
	(4) 虚线(厘米)	25.6	33.1	67.8	±∞	37.8	0.000	8.6	11.2	13.4	16.9	24.3
ω	(1) 转/分	2776	2830	2894	2895	3000	3009	3300	3500	3540	3600	3800
	(2) 弧度/秒	290.7	296.4	303.06	303.16	314	315.1	345.6	366.5	370.7	377	398
L_v	(5) 实线	150	−276	−47745	29882	166.9	152.7	41.6	27.3	25.5	23.2	16.5
	(6) 虚线	31.8	33.8	36.5	36.5	42.1	42.7	72.4	128.5	150	200.3	28293
ω	(1) 转/分	3802	4000	4106	4297	4393	4500	4640	4641	4730	4760	4830
	(2) 弧度/秒	398.2	419	430	450	460	471	485.9	486	495.3	498.5	505.8
L_v	(5) 实线	16.5	14.0	12.5	10.4	9.5	8.6	7.5	7.5	6.8	6.6	5.4
	(6) 虚线	141024	−263.1	−192	−159	−171	−229	193421	27995	213	147	78.8
ω	(1) 转/分	5000	5496.86	5800	6000	6095	6096	6150	6300	6500	7000	
	(2) 弧度/秒	524	575.63	607	628.3	638.27	638.37	644	660	681	773	
L_v	(1) 转/分	4.8	−0.000	−8.1	−40.4	−9208	9609	89.2	27.8	16.9	10.4	
	(2) 弧度/秒	26.2	−0.000	−3.2	−4.1	−4.4	−4.4	−4.6	−4.9	−5.1	−5.3	

Key: (1) revolutions/minute
(2) radians/second
(3) solid line (centimeter)
(4) dotted line (centimeter)
(5) solid line
(6) dotted line

imbalance on two different left and right balance planes. Therefore, the balancing speed of rotation of the part of the vibration center distance curve on the same side of the horizontal axis cannot be taken. The vibration center distance curve is on both sides of the horizontal axis but the solid line and the dotted line are asymmetric. The variation of the vibration center distance is larger. When the balancing speed of rotation is slightly unstable, or when the power source is unstable and cause the balanced speed of rotation to become unstable, variations in the vibration center distance will occur. The quality of balancing the rotor in these regions is poorer. The balancing speed of rotation in regions where the solid line and the dotted line of the vibration center distance curve are asymmetric about the horizontal axis also cannot be taken. In summary, the balancing speed of rotation taken should be within the region where the solid curve and the dotted curve are respectively on the two sides of the ω axis and are mutually symmetric about the ω axis. The speeds of rotation from 300 to 2,000 and greater than 7,000 can all be taken as the balancing speed of rotation.

VIII. Effect of Damping Upon the Quality of Balancing

To improve the precision of balancing by improving the stability of the vibration center distance of the vibration testing system, ordinarily the gyro rotor is balanced at its operating speed of rotation (high speed). To a sealed gyro rotor, the effect of damping is not great. But to an unsealed gyro rotor, the effect of damping on the quality of balancing should be taken into consideration. We know from vibration theory that damping has a visible effect upon amplitude and the phase angle. Figure 5 and Figure 6 show the characteristic curves of amplitude frequency and phase frequency of the vibrating system with one degree of freedom. D is the damping coefficient, ω is the rotary speed of the rotor, ω_n is the critical speed of rotation of the vibrating system, φ is the phase angle, V_1 is the ratio of amplitude to static positional change. The diagrams show that when the frequency ratio is fixed, the numerical values of the amplitude and the phase angle vary as the damping coefficient varies. Measurements of the amplitude and phase angle of a rotor being balanced at a balanced speed of rotation will be different if damping is different. Theoretically, a rotor being balanced at one speed of rotation should have the same amplitude and phase angle. But in actuality, the same rotor under different damping conditions will yield different measurements of amplitude and phase angle. This fact seriously affects the quality of balancing the rotor. To prevent the occurrence of this phenomenon, some measures should be taken: such as placing the rotor in a vacuum for balancing or balancing the rotor at high speeds and in high temperatures, or adjusting the mechanical system of the balancing machine so that the rotor is balanced within the stable regions of the characteristic curves of the amplitude frequency and the phase frequency.

XI. Several Sugrestions

1. When the rotor is being balanced on the balancing machine, the vibrating system moves about the vibration center. The distance between the vibration center and the center of mass of the rotor is called the vibration center distance. The vibration center distance is related to the system's rigidity, the

distance of the transducer to the center of mass of the rotor and the balanced speed of rotation. When the vibration center distance is zero, the vibrating system undergoes only angular vibration, the stationary imbalance on the rotor cannot be measured. When the vibration center distance approaches infinity, the vibrating system undergoes only linear vibration, and the dynamic imbalance on the rotor cannot be measured. These two situations should be avoided.

2. To avoid the two situations mentioned above, an appropriate balancing speed of rotation should be chosen. The balancing speed of rotation should be far away from the speed of rotation that produces the above phenomena.

3. Besides selecting an appropriate balancing speed of rotation, the rigidity of the vibrating system or the distance of the left and right transducers to the center of mass of the rotor can also be appropriately adjusted. Adjusting the rigidity and the transducers--distance from the center of mass can also produce a balancing speed of rotation that is far from the rotary speed of loss of vibration.

4. Damping affects the numerical values of the amplitude and the phase angle of the vibrating system relatively greatly. For some rotors of a higher precision, the effects of damping should be avoided in balancing. To realize this, balancing can be done in an environment where damping is very small.

5. Field balancing under operating conditions of the rotor is effective in improving the quality of balancing. Hard support balancing machines that do not use supports are also advisable.

REFERENCES

1. M. P. Kovalev, D. P. Morzhakov, D. C. Terehov: Dynamic Well-Balanced Rotor Gyroscopic System, 1962.

2. N. V. Kodeskich: Dynamic Well-Balanced Flexible Shaft, Heavy Machinery, No 5, 1962.

3. W. Kellenberger: Should a Flexible Rotor Be Balanced in N or Nt 2 Planes? A.S.M.E. Vibrations conference & international design automation conference Vol 1, 71--uibr--55, 1971.

4. R.E.D. Bishop and A.G. Parkinson: On the Isolation of Modes in the Balancing of Flexible Shafts. Proc lust; Mech. Engrs. Vol 177, No 16, pp 407-423, 1962.

5. R.E.D. Bishop and A.G. Parkinson: On the Use of Balancing Machine for Flexible Rotors. Trans. A.S.M.F. J. Eng. Industry Vol 94 (B2).

6. Collection of Materials on the Second National Dynamic Balance Conference, "Materials Testing Machines," 4-5, 1978.

7. F.M. Dimentberg: Bent Oscillating and Revolving Shaft.

9296
CSO: 8111/0228

MODEL-140 DEBUGGING PROGRAMS DETAILED

Liaoning ZHONGXIAOXING JISUANJI [MINI-MICRO SYSTEMS] in Chinese No 2, 25 Apr 80 pp 18, 29

[Excerpt]The model 140 machine has two debugging programs: a symbol debugging program III allowing interruption and a debugging program which does not allow interruption. They provide the user with a breakpoint facility for debugging his own programs and they provide partial printouts of some information, perform editing and search functions for specific commands or data to monitor and control the user's programs.

Assembly programs provide the function to connect and assemble each program. It can assemble certain floating binary documents and stored documents into executable stored documents. The assembly program can also be used to create user overlays.

The above compiler programs and service programs can operate under all kinds of operational systems. The following two service programs are provided for binary forms and can be used independently.

Duplicate paper tape programs can duplicate any type of binary paper tape and can be used to check on the accuracy of new duplicating paper tape.

Magnetic disc editing programs can be used to directly edit or restore certain messages in the index magnetic disc, and thus restore documents on magnetic discs that have not been destroyed.

4. Auditing and Diagnostic Programs

To coordinate with the debugging and maintenance of hardware, the 140 machine is equipped with various kinds of auditing and diagnostic programs. These programs can find malfunctions for the debugger and can carry out error registration correctly to pinpoint the malfunctioning part. The auditing and diagnostic programs of the 140 machine include: CPU logic diagnostic program, arithmetic auditing program, internal storage auditing programs I, II, III, basic peripheral auditing program, complete practice auditing program, power source cutoff and start up and restart up auditing program, teletypewriter auditing program, paper tape input auditing program, paper tape puncher auditing program, character display auditing

program, digital plotter auditing program, wide line printer auditing program, real time clock auditing program, internal management and maintenance parts auditing program, QTY multiplex auditing program, floating point computation components auditing program, movable head magnetic disc logic diagnostic program, movable head magnetic disc reliability auditing program, fixed head magnetic disc logic diagnostic program, fixed head reliability auditing program, magnetic tape drive logic diagnostic program, magnetic tape drive reliability auditing program, miniature magnetic tape drive logic diagnostic program, minature magnetic tape drive reliability auditing program and multiple I/O equipment reliability auditing program.

III. Program Storage and Program Package

The 140 machine is equipped with a floating point interpretive program, FORTRAN operation program (storage and data plotting program package (DATA PLOT)) and it is also equipped with other kinds of application software and program packages.

1. The floating point interpretation package. This enables the machine to perform various kinds of operations and computations of floating point numbers by software when the floating point unit (FPU) is not available.

2. FORTRAN operational program storage. This provides a complete set of subroutines for the various kinds of data formates, multiple computations of character strings and for using multiple task systems of documents, equipment and indexes.

3. Data plotting package. This provides a series of standard subroutines for a systematic use of the plotter, such as plotting coordinates, origin and lines.

4. Buffer input/output package (BFPKG). It enables one to use the buffer processing method to increase the processing efficiency of the I/O equipment. The use of the various kinds of OPEN, READ/WRITE and CLOSE commands provided by this program package can replace the READ/WRITE commands of related documents in RDOS and MRDOS, at a higher processing speed.

5. Scientific computation package I, II. These are standard subroutines of many frequently used computational methods used in scientific, technological and engineering computations. NSPI includes various types of matrix computations, ordinary differential equations, numerical differentiation and numerical integration totaling 10 standard programs. NSPII includes multiple regressive analysis, correlation analysis and various types of statistical analysis programs totaling 12 programs.

6. Discrete Fourier Transform. This is a data processing method often used in scientific and technological computations. This program package provides a software subroutine for that method of computation.

IV. Application of the DJS140 Machine

The DJS140 is a small sized general purpose digital computer of multiple functions. It is suitable for use in various types of real time process controls and medium and small scale scientific and technological computations:

1. Real Time Process Control. To adapt to real time processing demands, the 140 machine has been designed to possess real time clocks of various clock frequencies and the capability to respond to the data channels in the course of execution of commands. The functions of channel plus "1" and channel add have provided an important means for carrying out computations of probabilities of the data collected during the course of real time processing. The software systems of the 140 machine are completely oriented towards real time applications, such as real time FORTRAN and real time operating systems. The 140 machine can be equipped with a digital-analog (DA) and analog-digital (AD) converter and a process input/output system (PIO), which can be used to monitor, control and manage production processes.

2. Scientific and Technological Computations. The 140 machine's floating point unit can perform computations of 14 to 15 significant digits of the decimal system. This basically satisfies the ordinary demands of engineering and scientific and technological computations. The 140 machine also provides the user several more commonly used computational languages, such as BASIC, ALGOL 60, FORTRAN. The systems software of the 140 machine are not extensive but are representative. Thus they are better suited for use as teaching materials for institutes of higher learning to establish computer centers. At present, writing of a lot of teaching materials by the computer staff of the nation's scientific and engineering fields has combined the systems software of the 100 series machines.

3. Data Processing. The 140 machine has provided a medium for large capacity storage of documents and large amounts of data on magnetic disc and magnetic tape storage systems. The documentation system and other related programs can perform such functions as collecting, storing, transmitting, classifying and various output processing of all kinds of data. The system can also provide corresponding management programs and software packages for asynchronous multiplexors and far end users to realize real time or time shared management by the user of the terminals.

4. Processing of Graphs. The 140 machine is equipped with graphic output equipment, such as digital plotter and corresponding software (such as DATA PLOT programs package). The 140 machine can perform refining and processing of many kinds of graphs.

5. Multiple machine systems and networks. The 140 machine is equipped with a machine-machine trunk line drive that enables duplex operation of duplex machines or dual processing by duplex machines. The two machines can work independently while using the same magnetic disc as when a duplex computer system shares a magnetic disc for communication between programs. When only one machine malfunctions, the other standby machine can switch over to continue to perform the processing function. Two machines can also share the load of processing by working as a duplex. All of these methods can increase the reliability

of the system or expand the processing capabilities of the system. The multiple processor's communications converter of the 140 machine provides connection and communication among as many as 15 comp' .ers, forming a multiple machine system. The 140 machine is also equipped with special interfaces and corresponding program packages that can interface with IBM series machines. This makes the 140 machine easy to expand into a multiple machine system or to be connected to a computer network.

At present, the 140 machine is being mass produced by the Beijing Computer Plant No 3, Jinzhou Radio Plant No 2 and Liaoyuan Radio Plant No 3.

9296
CSO: 8111/0206

PUBLICATIONS

TABLE OF CONTENTS OF 'JICHUANG' NO 2, 1980

Beijing JICHUANG [MACHINE TOOL] in Chinese No 2, Feb 80 p 1

[Text] Comments on Special Topics

9717
CSO: 4008

PUBLICATIONS

TABLE OF CONTENTS OF 'TIANWEN XUEBAO' NO 3, 1980

Beijing TIANWEN XUEBAO [ACTA ASTRONOMICA SINICA] in Chinese Vol 21 No 3, 1980 inside back cover

9717
CSO: 4008

PUBLICATIONS

TABLE OF CONTENTS OF 'JISUANJI XUEBAO' NO 4, 1980

Beijing JISUANJI XUEBAO [CHINESE JOURNAL OF COMPUTERS] in Chinese Vol 3 No 4, 1980 on back cover

9717
CSO: 4008

PUBLICATIONS

TABLE OF CONTENTS OF 'ZIDONGHUA XUEBAO' NO 4, 1980

Beijing ZIDONGHUA XUEBAO [ACTA AUTOMATICA SINICA] in Chinese No 4, Oct 80 inside back cover

9717
CSO: 4008

PUBLICATIONS

TABLE OF CONTENTS OF 'HAIYANG YU HUZHAO' NO 4, 1980

Beijing HAIYANG YU HUZHAO [OCEANOLOGIA ET LIMNOLOGIA SINICA] in Chinese Vol 11 No 4, Oct 80 inside back cover

9717
CSO: 4008

PUBLICATIONS

TABLE OF CONTENTS OF 'GAOFENZI TONGXUN' NO 5, 1980

Beijing GAOFENZI TONGXUN [POLYMER COMMUNICATIONS] in Chinese No 5, 1980 inside back cover

[Text] Papers

9717
CSO: 4008

PUBLICATIONS

TABLE OF CONTENTS OF 'DIANZI SHIJIE' NO 6, 1980

Beijing DIANZI SHIJIE [ELECTRONIC WORLD] in Chinese No 6, Jun 80 p 1

[Text] Table of Contents

9698
CSO: 8111

PUBLICATIONS

TABLE OF CONTENTS OF 'HUAXUE TONGBAO' NO 9, 1980

Beijing HUAXUE TONGBAO [CHEMISTRY] in Chinese No 9, 1980 on back cover

9717
CSO: 4008

PUBLICATIONS

TABLE OF CONTENTS OF 'DIANXIN JISHU' OCTOBER 1980

Beijing DIANXIN JISHU [TELECOMMUNICATIONS TECHNOLOGY] in Chinese No 10, Oct 80
Inside back cover

[Text] Table of Contents

9698
CSO: 4008

AUTHOR: ZHAO Guotan [6392 0948 5672]
GAO Junsheng [7559 0193 0581; deceased]
LI'O Wanqing [1675 1238 0615]
WA.G Qingxiang [3769 3237 3276]

ORG: All of Dalian Institute of Technology

TITLE: "Experiments and Calculating Method for the Cracking Strength and the Maximum Crack Width in Reinforced Concrete Members"

SOURCE: Beijing JIANZHU JIEGOU XUEBAO [JOURNAL OF BUILDING STRUCTURE] in Chinese Vol 1 No 4, 5 Nov 80 pp 1-17

TEXT OF ENGLISH ABSTRACT: The experiments and data of reinforced concrete members subjected to bending, eccentric compression and eccentric tension are presented in this paper. Discussions are made on the equations for calculating the cracking strength of reinforced concrete members and the parameter γ involved in these equations to consider the plastic behavior of the tension zone.

A formula for calculating the value of γ and an empirical formula for calculating the maximum crack width in reinforced concrete members are proposed. The recommended formulas are verified with test data obtained from the research work of DIT and other institutes.

AUTHOR: LIANG Dahua [5592 1129 7520]
LIANG Mintao [2733 2404 3325]

ORG: LIANG of Tongji University; LIANG of the Second Design Institute, Ministry of Agricultural Machinery

TITLE: "Flexural Strength of Single Footing and Innovation in the Arrangement of Reinforcement"

SOURCE: Beijing JIANZHU JIEGOU XUEBAO [JOURNAL OF BUILDING STRUCTURE] in Chinese Vol 1 No 4, 5 Nov 80 pp 18-27

TEXT OF ENGLISH ABSTRACT: Several upper and lower bound solutions based on the theory of plasticity for the flexural strength of single footing under column load are presented. The results show that the formula used in current practice for determining the area of reinforcement is unsafe and a more reasonable one is recommended. Instead of the rectangular net usually used in practice, the use of more economical circumferential reinforcement for the footing is suggested in this paper, which would save nearly 20 percent reinforcement. Test results are also reported.

AUTHOR: DING Yunsun [0002 0061 1327]
HU Caiyuan [5170 2088 3293]

ORG: Both of the Fourth Planning Design and Research Institute, Third Ministry of Machine Building

TITLE: "A 54 x 48 m Space Truss Roof Hangar"

SOURCE: Beijing JIANZHU JIEGOU XUEBAO [JOURNAL OF BUILDING STRUCTURE] in Chinese Vol 1 No 4, 5 Nov 80 pp 28-32

TEXT OF ENGLISH ABSTRACT: A space truss roof hangar with three sides supported and one side free is reported in this paper. The structural pattern used for the space truss roof was inclined square mesh with lower chords parallel to the boundaries. A stiffening girder was used on the free side, i.e., an additional layer of inclined square mesh was installed on the top of the space truss within the two panels along the door opening. A strengthening effect was provided by the stiffening girder, so that the space truss beyond the stiffening girder is acting as if it is being supported along four sides.

The entire roof structure was assembled on the ground and raised with hydraulic jacks which were used for lifting the slip forms of the concrete columns. The slip forms and the raising of the space truss proceeded simultaneously and satisfactory results were obtained.

AUTHOR: CHEN Yongchun [7115 3057 2504]
et al.

ORG: All of Wuxi Building Construction Bureau, Chinese Academy of Building Research, Jiangsu Building Research Institute

TITLE: "Multistory Factory Building System of Longitudinal Frames Using Lift-Form Technique"

SOURCE: Beijing JIANZHU JIEGOU XUEBAO [JOURNAL OF BUILDING STRUCTURE] in Chinese Vol 1 No 4, 5 Nov 80 pp 33-37

TEXT OF ENGLISH ABSTRACT: A new longitudinal frame building system with lift-form technique for the construction of multistory factories is presented in this paper. In this system, the frames and wall panels are constructed by means of the lift-form casting; along the exterior longitudinal frames the girders serve both as load bearing beams and walls. Only light lifting equipment (i.e., tower crane of 25 t-m) are needed for constructing five-story or taller factory buildings. The design and construction practice of three multistory factory buildings in Wuxi has shown that a fast speed in construction and good technical and economical results were attained by the use of this system.

AUTHOR: WU Qiyun [0702 4860 5366]
TIAN Jiahua [3944 1367 7520]
XU Xianyi [1776 7359 3015]

ORG: All of the Chinese Academy of Building Research and Beijing Polytechnical University

TITLE: "A Study of the Behavior of Brick Infilled Frame Structures under Monotonic and Reversed Cyclic Horizontal Loads"

SOURCE: Beijing JIANZHU JIEGOU XUEBAO [JOURNAL OF BUILDING STRUCTURE] in Chinese Vol 1 No 4, 5 Nov 80 pp 38-44

TEXT OF ENGLISH ABSTRACT: Based on the experimental study of the process of working stages to failure of reinforced concrete frame structures infilled with brick walls under monotonic and reversed cyclic horizontal loads and analyses of their properties on deformation and destruction, formulae for calculating the ultimate strength and stiffness at three different working stages are given in this paper. The results obtained from computation and tests show reasonable agreement in comparison. Furthermore, the restoring force characteristic model and elastoplastic characteristic parameters of the structural members of this kind of structure are also given in the paper.

AUTHOR: XU Zuzhen [6877 3419 3791]

ORG: Chinese Academy of Building Research

TITLE: "Calculation Methods of Strengthening and Repair of Brick Masonry Structures for Earthquake Resistance"

SOURCE: Beijing JIANZHU JIEGOU XUEBAO [JOURNAL OF BUILDING STRUCTURE] in Chinese Vol 1 No 4, 5 Nov 80 pp 45-54

TEXT OF ENGLISH ABSTRACT: Calculating methods of strengthening and repairing measures of brick masonry structures are described in this paper. These methods are based on the available testing data of the institutes concerned. The strengthening and repairing measures used are as follows:
1. Cement mortar coating, reinforced cement mortar coating attached to the wall surfaces or reinforced concrete columns with tie beams were used for strengthening walls.
2. Reinforced cement mortar attached to the surface or steel angles at the corners were used for strengthening columns.
3. Vertical and circular steel strips attached to the surface were used for strengthening the walls.

This paper shows that the results calculated by these methods are closer to the testing data than are those calculated by the currently available methods.

AUTHOR: JIANG Daixin [0781 1486 2450]
LUO Weiqian [5012 4850 0467]
MENG Xianjun [1322 2009 0689]

ORG: All of Harbin Institute of Civil Engineering

TITLE: "The Testing and Analysis of Local Bearing Strength of Brick Masonry"

SOURCE: Beijing JIANZHU JIEGOU XUEBAO [JOURNAL OF BUILDING STRUCTURE] in Chinese Vol 1 No 4, 5 Nov 80 pp 55-63

TEXT OF ENGLISH ABSTRACT: Several sorts of basic failure mechanism of local bearings of brick masonry are observed through many tests. Together with the analysis of the computed results obtained from a computer, the actual working behavior of local bearing of brick masonry is presented. The problems existing in the formula in the current code for calculating the local bearing strength of brick masonry are then studied and a practical formula conforming more to real conditions is suggested in this paper.

AUTHOR: ZHANG Wenqing [1728 0795 3237]
ZHAO Xitong [6392 6932 1347]

ORG: Both of Tongji University

TITLE: "A Step-by-Step Extended Substructure Model for Computing the Stiffness of Tall Buildings"

SOURCE: Beijing JIANZHU JIEGOU XUEBAO [JOURNAL OF BUILDING STRUCTURE] in Chinese Vol 1 No 4, 5 Nov 80 pp 66-70

TEXT OF ENGLISH ABSTRACT: In applying the conventional substructure method to tall-building interaction, the number of structural elements always exceeds the capacity of available computer programs. For this purpose, a step-by-step (story-by-story, bay-by-bay or joint-by-joint) extended substructure method is presented in this paper. By comparison, it has an advantage over the routine substructure method.

AUTHOR: FANG Shimin [2455 0013 2404]

ORG: Shanghai Municipal Institute of Civil Architecture Design

TITLE: "The Use of Substructural Analysis Method for Superstructure-Foundation Interaction"

SOURCE: Beijing JIANZHU JIEGOU XUEBAO [JOURNAL OF BUILDING STRUCTURE] in Chinese Vol 1 No 4, 5 Nov 80 pp 71-79

TEXT OF ENGLISH ABSTRACT: In this paper the principle of substructure analysis of matrix displacement method is used to condense superstructural stiffness of tall buildings to the boundary stiffness of the foundation beams, and the subsoil model of the layers summation procedure of the finite compressible layer is introduced herein. The flexibility matrix of the subsoil at the interface is attained by means of the integral transformation of settlement at the interface of the subsoil acting with rectangular loading. When conditions of the deflection compatibility and the boundary restraint at the interface are satisfied, a set of matrix equations of displacement of the foundation beam is made, which is equivalent to the actual conditions, and the calculation is simplified in this way. In the paper, numerical examples are provided as well.

9717
CSO: 4009

AUTHOR: LIU Hongyun [0491 7703 0336]
DONG Rongsheng [5516 2827 3932]
LI Jianlin [2621 1696 2651]
YANG Yanjun [2799 1750 0971]

ORG: LIU of the Institute of Geology, Chinese Academy of Sciences; LI and DONG both of Chengdu Institute of Geology, YANG of the Regional Geologic Survey Team of Hunan Geology Bureau

TITLE: "Problems of Classification and Correlation of the Sinian System"

SOURCE: Beijing DIZHI KEXUE [SCIENTIA GEOLOGICA SINICA] in Chinese No 4, 1980 pp 307-321

EXCERPT FROM ENGLISH ABSTRACT: There exists a number of problems in the Sinian system research, especially the stratigraphic classification and correlation, which need to be inquired into and discussed deeply and repeatedly. The present paper lays emphasis on the argument concerning the scope, diverse facies, principle of classification and correlation of some representative lithostratigraphic units of the Sinian system.

AUTHOR: LI Congxian [2621 1783 0341]
WANG Jingtai [3769 7231 3141]
XU Shiyuan [6079 0013 6678]
et al.

ORG: All of the Department of Marine Geology, Tongji University

TITLE: "Holocene Transgressive-Regressive Sequence in the Changjiang Delta Area"

SOURCE: Beijing DIZHI KEXUE [SCIENTIA GEOLOGICA SINICA] in Chinese No 4, 1980 pp 322-330

TEXT OF ENGLISH ABSTRACT: The Changjiang delta area has undergone a transgression caused by postglacial rapid rise in sea level and regression resulting from delta progradation. Consequently, the Holocene lithofacies relationship may be grouped into transgressive and regressive sequences. The transgressive-regressive sequence in the delta plain of the Changjiang consists of transgressive channel-fill sequence and overlying deltaic sequence. On the strandplain the transgressive sequence is composed mainly of barrier-lagoonal deposits; the regressive sequence consists of radiated bar sedimentary complex on the northern flank of the Changjiang and of progradation of tidal flat on the southern flank.

Transgressive-regressive sequences in the Changjiang delta area show a distinct cyclothem in ascending order: the variation in grain size is coarse-fine-coarse;

[Continuation of DIZHI KEXUE No 4, 1980 pp 322-330]

facies relationship: littoral-shallow marine-littoral; apparent resistivity pattern--high-low-high; climate referred by sporal-pollen assemblage is cold-temperate-cool. The changes of these features can be correlated fairly well with each other.

With the alternation of transgression and regression the sand bodies are characterized by double beds in vertical distribution. The transgressive sand bodies are overlain by the regressive ones, and between them exists a wedge marine clay.

AUTHOR: LUO Yinding [4382 6855 6928]
YAN Qingnan [6768 1987 0589]

Org: LUO of the Department of Mining and Metallurgy, University of Fuzhou; YAN of the Regional Geological Survey Team, Geological Bureau of Fujian

TITLE: "On the Horizon and the Age of Main Seam of Makeng Type Iron Deposits in Southwestern Fujian."

SOURCE: Beijing DIZHI KEXUE [SCIENTIA GEOLOGICA SINICA] in Chinese No 4, 1980 pp 331-339

EXCERPT FROM ENGLISH ABSTRACT: A careful study of the profile exposed in the Lufong area of Shanghang district has enabled the authors to draw a new detailed section to systematically show the Carboniferous stratigraphical sequence of Fujian Province. It is shown by examining the outcrops and cores that the main seam of Makeng type iron deposits, occurring in the Longyan and Shanghang districts of southwestern Fujian, lies disconformably on the Lindi Formation and is overlain conformably by Huanglong beds. Recent studies on the fossils collected from the overlying and underlying strata afford the evidence to determine the horizon and the age of the main seam of iron deposits.

AUTHOR: ZHANG Qi [1728 2475]
ZHANG Zhenyu [1728 2182 4416]
LI Shaohua [2621 8734 5478]

ORG: None

TITLE: "Muscovite of Metamorphic Rocks in East and South Xizang and Its Petrological Significance"

SOURCE: Beijing DIZHI KEXUE [SCIENTIA GEOLOGICA SINICA] in Chinese No 4, 1980 pp 340-347

TEXT OF ENGLISH ABSTRACT: In this paper, the authors deal with nine samples of muscovite collected from Xizang, China. The X-ray powder diffraction pattern of the muscovite indicates that its b_0 value varies with the metamorphic pressure, i.e., the higher the pressure is, the larger the b_0 value is, thereby serving as an indicator of metamorphic pressure. However, d_{002} decreases with the increase of pressure. Obviously, the high pressure condition favors the formation of muscovite with small basal spacing and large horizontal spacing. Likewise, the mineral composition of muscovite can also be correlated to a certain extent with the metamorphic pressure. MgO in muscovite may be taken as a particularly good indicator of metamorphic pressure. The authors suggest that two types of original rock series, i.e., metapelites and metabasites, can be recognized. Therefore, diagrams of MgO vs RM and Si vs Mg of the muscovite-phengite series of greenschist-glaucophane schist facies were constructed by the present authors and are presented in this paper. Two

[Continuation of DIZHI KEXUE No 4, 1980 pp 340-347]

areas, medium pressure facies series areas and high pressure facies series areas, are distinguished. The latter can be further subdivided into Area I, which contains glaucophane assemblages, and Area II, which contains no glaucophane assemblages. The samples from Yarlung Zangbo Jiang metamorphic belt in Xizang fall into the field of Area II.

AUTHOR: CHEN Jishi [7115 3423 4258]

ORG: None

TITLE: "The Old Tidal Deposits in the Xuanhua Area, Hebei Province"

SOURCE: Beijing DIZHI KEXUE [SCIENTIA GEOLOGICA SINICA] in Chinese No 4, 1980 pp 348-355

TEXT OF ENGLISH ABSTRACT: About 1.8 b.y. ago, the marine transgression taking place in the Xuanhua area, Hebei Province, transformed this area into a bay opening toward the east and extending east-west. The marine terrigenous clastic sediments with a thickness of approximately 200 m were deposited there. The various types of primary sedimentary structures marking clastic tidal environment are well developed in these sediments, such as herringbone cross-bedding, lenticular bedding, wavy bedding, flaser bedding, beach cross-bedding, tidal channel and tidal channel fill of cross-bedding, reactivation surfaces, interference ripple marks, mud cracks, and pene-contemporaneous deformation structure. This paper makes a brief discussion of the origin and distribution of these sedimentary structures.

Based on lithological characteristics and succession, the primary sedimentary structures and their sequences, as well as the grain size distribution of sediments, the late Precambrian tidal depositional environment in this area can be subdivided as follows: tidal flat (high-tidal flat, mid-tidal flat and low-tidal flat), sandy

[Continuation of DIZHI KEXUE No 4, 1980 pp 348-355]

beach, algal flat and oolitic bank, and shallow sea. Moreover, the main sedimentary features of these sub-environments are described and two types of depositional models for the area studied are proposed. Finally, paleocurrent regime is also briefly investigated.

AUTHOR: WEI Mingxiu [7614 2494 4423]

ORG: Institute of Geology, Ministry of Metallurgy

TITLE: "Unit Cell Constant and Genetic Character of Chrome Spinels"

SOURCE: Beijing DIZHI KEXUE [SCIENTIA GEOLOGICA SINICA] in Chinese No 4, 1980 pp 356-367

TEXT OF ENGLISH ABSTRACT: The unit cell constant (a), specific gravity (G), reflectivity (R), microhardness (H) and chemical composition of 30 chrome spinel samples from deposits of different genesis in China were determined. Based on crystallo-chemical properties, a new formula for the unit cell constant of chrome spinels is proposed: $a = 8.367\ \text{Å} - 0.01745\ (Al^{+3})\text{Å}$, where (Al^{+3}) is the number of Al^{+3} in the unit cell. It is more accurate than Mikheev's formula. The composition of chrome spinel could be calculated directly from its unit cell constant by the formula: $(Al^{+3}) = 479.45 - 57.3a$. Based upon the theoretical calculation, a new curve showing the relation between sp. gr. and composition is plotted. From the above relationship it is easy from a and G to derive the crystal chemical formula: $R^{+2}_{8}\ (Mg^{+2}, Fe^{+2})\ R^{+3}_{16}\ (Al^{+3}, Cr^{+3} + Fe^{+3})\ O_{32}$. A tetragonal composition diagram Mg^{+2}-Fe^{+2}-Al^{+3}-$(Cr^{+3}+Fe^{+3})$ of chrome spinels constructed from a and G is also given. It is clearly shown that the chrome spinel of the geosynclinal type (Alpine type) is quite different from that of the platform type (or stratiform type). A simplified

[Continuation of DIZHI KEXUE No 4, 1980 pp 356-367]

classification method for chrome spinel groups is proposed. "Molecular Iron Content F_{Cr}" is probably an important factor of metallogenetic process and can be used as an indicator for the enrichment of chromite ore. Finally, some mineralogical characters of the chrome spinels associated with platinum deposits are discussed.

AUTHOR: [illegible] [1327 1639 1813]
ZHOU Ruiquang [0719 3843 0342]

ORG: None

TITLE: "The Structural Effect of Rockmass Deformation and Failure"

SOURCE: Beijing DIZHI KEXUE [SCIENTIA GEOLOGICA SINICA] in Chinese No 4, 1980 pp 368-376

TEXT of ENGLISH ABSTRACT: The rockmass strength of jointed sedimentary rock often shows a distinct scale effect. In fact, it is a reflection of the rockmass structure effect. This view has been confirmed by our tests on the pressure-resistance of jointed slates in situ. Moreover, the results from these tests with jointed slate specimens of different sizes in situ indicate that the pressure-resistance strength of the rockmass is distinctly related to the number of structure bodies in the test-piece rather than to the size of specimens. Taking into consideration the results of tests and using a statistical method, we found that the relationship between the uniaxial compression strength of slate rockmass and the structure bodies number N in test specimens can be expressed as $\delta_m = 24 + 236N^{-0.36}$.

AUTHOR: [illegible] [1492 1987 3012]

ORG: [illegible], Shanxi Designing Institute of Water Conservancy and [illegible] Power

TITLE: "[illegible]-shaped Structure and Its Characteristics of Engineering [illegible] of Rock Mass"

SOURCE: Beijing DIZHI KEXUE [SCIENTIA GEOLOGICA SINICA] in Chinese No 4, 1980 pp [illegible]

[illegible]: Based on field investigations and the results of rock [illegible], the [illegible]-shaped structure and its engineering geo[illegible] of rock mass are discussed in this papet.

. [illegible] of jointed structure is a small swirling structure which consists of [illegible] under repeated torsional compression forces;

. [illegible]-shaped structure, different types of rock mass structures show [illegible] which are usually controlled by both whirl planes [illegible]. Each type of rock mass structure has its own mechanical characteristics;

. [illegible] of rock masses in the torus-shaped structure, four zones but [illegible] can be distinguished: elastic deformation zone, quasi-elastic deformation zone, elasto-plastic deformation zone and plastic deformation zone;

[Continuation of DIZHI KEXUE No 4, 1980 pp 377-385]

4. Both the nuclear pillar and the central parts of the whirling strata within the lotus-shaped structure are favorable regions of engineering geomechanical conditions, i.e., the elastic and quasi-elastic deformed zone; the marginal parts of the whirling strata, i.e., elasto-plastic deformed zone, are the less favorable regions, and all of the plastic deformed zone in the whirling planes is the unfavorable region.

AUTHOR: [illegible]

ORG: Nanjing Geological Institute of Geology and Mineral Resources, Chinese Academy of Geological Sciences

TITLE: "About a Method for Calculating the Cell Dimensions of Low Symmetrical Rock-forming Minerals"

SOURCE: Dizhi Kexue [SCIENTIA GEOLOGICA SINICA] in Chinese No 4, 1980 pp [illegible]

[TEXT OF ENGLISH ABSTRACT]: In this paper, the author proposes a method for calculating the cell dimensions of low symmetrical rock-forming minerals on the basis of determinating data of their X-ray powder patterns. This method is applicable to the data obtained both by the diffractometer and the 57.3 cm powder camera. In fact, it is a computing process based on a weighted least-square fitting combined with successive indexing by iteration. A computer program in ALGOL 60 language has been written by the author and has been successfully run on a 709 computer.

AUTHOR: BIE Wanli [0446 1238 3829]
DONG Guangtu [5516 0342 1788]

ORG: None

TITLE: "Semimicro-analysis of Fluorine in Minerals by a Method of Fluorine-Ion Selected Electrode"

SOURCE: Beijing DIZHI KEXUE [SCIENTIA GEOLOGICA SINICA] in Chinese No 4, 1980 pp 399-402

TEXT OF ENGLISH ABSTRACT: This paper introduces a method for directly determining fluorine without any separation procedure. It can be used in the presence of ethyl alcohol, and potassium citrate as ionic strength adjustment buffer (pH 6-6.5). The determinations indicate that this method has some advantages, such as high sensitivity and the Nernst linear extent up to 1×10^{-1} M - 1×10^{-6} M, one order higher in magnitude than the usual ones. Moreover, the method proposed here requires samples smaller in amount (1-5 ml). In general, it is applicable for determining fluorine in minerals.

AUTHOR: PEI Jingxian [5952 7234 1288]

ORG: None

TITLE: "Thermoluminescence Datings of the Cave Deposits in Zhoukoudian and the Volcanic Ash Baked Layer in Datong, Shanxi Province"

SOURCE: Beijing DIZHI KEXUE [SCIENTIA GEOLOGICA SINICA] in Chinese No 4, 1980 pp 403-409

TEXT OF ENGLISH ABSTRACT: The thermoluminescence datings of some samples collected from the Zhoukoudian cave and the volcanic areas in Datong are given in this paper.

The cave deposits of Upper Cave in Zhoukoudian give the ages ranging from 33,000 yr B.P. for the upper limit to 49,000 yr B.P. for the lower limit, while the ash of new caves has an age of 0.25 ± 0.03 m.y. The age determinations of these samples indicate that the volcanic activity in western Datong ceased early, while in eastern Datong it lasted longer, up to more than 100,000 years ago. These results are in close agreement with the conclusion given by Professor YIN Zanxun [1438 6363 0534] (1976).

AUTHOR: CHEN Meng'e [7115 1322 5458]
CHEN Yiyuan [7115 2011 0337]

ORG: CHEN Meng'e of the Institute of Geology, Chinese Academy of Sciences; CHEN Yiyuan of Wuhan Geological College

TITLE: "Note on Possible Coprolites from the Lowest Cambrian Strata of the Changjiang Gorge"

SOURCE: Beijing DIZHI KEXUE [SCIENTIA GEOLOGICA SINICA] in Chinese No 4, 1980 pp 406-407

TEXT OF ENGLISH ABSTRACT: The paper describes a kind of possible coprolites from lowest Cambrian (equivalent to the Tommotian stage) strata, the Tian-Zhu-Shan member of the Dengying Formation of the Changjiang Gorge. These fossils are small (length about 1 mm), coprolitic or intestinally convoluted and irregularly curved in structure, gray and smooth. The original constitution of these fossils is unknown, but now they are made up of phosphate. This coprolite evidently is derived from a coelomate. Therefore, it is suggested that the convoluted-form coprolite appeared in ancient strata along with the ellipsoid-form coprolite. This fact is of not only paleontological, but also sedimentological significance.

9717
CSO: 4009

AUTHORS: SHAO Binxiu [0730 3521 4872]
WANG Chaoxie [3769 2490 3610]
HUANG Cuifang [7806 5050 5364]

ORG: All of the Department of Biology, Fudan University

TITLE: "The Influence of Environmental Salinity on the Prolactin and Gonadotropin Secretory Regions in the Pituitary of Trachidermus fasciatus"

SOURCE: Beijing HAIYANG YU HUZHAO [OCEANOLOGIA ET LIMNOLOGIA SINICA] in Chinese Vol 11 No 4, Oct 80 pp 314-319

TEXT OF ENGLISH ABSTRACT: Trachidermus fasciatus is a kind of catadromous fish in China. In order to study the reasons for its seaward propagation, comparative study of the pituitaries of this fish collected from both freshwater and seawater (salinity 30-32 percent) in the breeding season was done from 1978 to 1979. The volumetric and histological changes in the rostral and proximal pars distalis of their pituitaries are now described as follows.

In the environment of different salinities, the most pronounced changes occurred in the size of the rostral pars distalis and proximal pars distalis of the pituitaries. The rostral pars distalis, in which the main component is the prolactin secretory region, occupies 33.52 percent of the adenohypophysis in the fish collected from freshwater, and this percentage drops to 19.48 percent in those collected from seawater. The volumetric change of the proximal pars distalis is the inverse of that

[Continuation of HAIYANG YU HUZHAO Vol 11 No 4, Oct 80 pp 314-319]

of the rostral pars distalis. The proximal pars distalis, which contains the gonadotropic secretory region, occupies 48.10 percent of the adenohypophysis in the fish collected from freshwater and goes up to 58.04 percent in those collected from seawater.

The volume of the prolactin cells in the rostral pars distalis shows evident [illegible] to environmental salinity and the increase [illegible]. The basophilic prolactin cells are oval and highly vacuolated. Cells of the fish collected from freshwater and do not exhibit definite boundaries. The prolactin cells of the fish collected from seawater show signs of involution. The cells become smaller and the number of secretory granules decreases. The boundaries of the cells are clearly defined. Prolactin is an anti-gonadotropin agent. Therefore, in the fish collected from freshwater, the basophilic gonadotropic cells in the proximal pars distalis are smaller and the secretory granules of the cells are few, while in the fish collected from seawater the gonadotropic cells become larger and the amount of secretory granules of the cells increases. This phenomenon illustrates that the increase of the environmental salinity can retard the secretion of prolactin cells and then improve the secretion of gonadotropic cells. [illegible] ready for the infertility of Trachidermus fasciatus confined to freshwater. Therefore, Trachidermus fasciatus must migrate to the sea to spawn.

AUTHOR: LI Wenzhi [2621 2773 3365]
SUN Renyi [0656 0088 3030]
MENG Zhaocai [1322 2507 2008]

AFFIL: All of the Institute of Oceanology, Chinese Academy of Sciences

TITLE: "On the Absorption of Ammonium Nitrogen by Porphyra yezoensis Ueda. I. The Effects of N-Concentration and Aeration on the Rate of Absorption"

SOURCE: HAIYANG YU HUZHAO [OCEANOLOGIA ET LIMNOLOGIA SINICA] in Chinese Vol 11 No 4, Oct 80 pp 358-361

TEXT OF ENGLISH ABSTRACT: An investigation on the absorption of ammonium nitrogen under low concentration (ranging from 100 μg/l to 1500 μg/l) by using the intact frond of Porphyra as experimental material has been carried out. The results concerning the effect of N-concentration and aeration on the rate of absorption and the time course are summarized as follows.

Fronds (pieces) of Porphyra can exhaust ammonium nitrogen in a medium (400 ml) with a concentration of 100 μg/l in about two hours. The results indicate that the absorption ability of Porphyra is rather strong. The rate of absorption remained unchanged during the first 90 minutes. This suggests that the changing of concentration seems to have no effect on the rate of absorption.

[Continuation of HAIYANG YU HUZHAO Vol 11 No 4, Oct 80 pp 358-361]

In a strongly aerated media, the absorption plateau appeared in about 200 μg/l, whereas in weakly or non-aerated media the plateaus appeared in rather high concentrations. The heights of plateaus of different aerated media are more or less similar. These results suggest that aeration plays a stirring role which increases the chance of contact between the NH_4^+ ions and the surface of Porphyra.

It is concluded that the absorption of ammonium nitrogen by frond is an active absorption process.

REF: 7
TAB: 4 ILL: 4

AUTHOR: WANG Xinwu [3769 2450 0710]

ORG: None

TITLE: "Characteristics of the Activity of the Xianshui River Fault"

SOURCE: Beijing DIZHEN ZHANXIAN [SEISMOLOGY FRONT] in Chinese No 2, 26 Mar 80 pp 5-6

ABSTRACT: The Xianshui River fault runs roughly northwest and southeast, intersecting a number of other faults. The fault surface is generally inclined toward the northeast, with an angle of 60-80 degrees. There is a fracture zone of about 20-300 meters in width. A network of 7 stations distributed on both sides of the fault was set up and vertical and horizontal position readings taken starting in 1973-74. Measurements taken following the 1973 Luhuo earthquake indicate that the block southwest of the fault is sinking and that northeast of the fault rising. But movement is not uniform, and measurements presented show that the Luhou area is one of high activity (energy release). The area to the south of Daofu station shows little activity, indicating that stress is likely to be building up. Similar results are found for horizontal displacement. If the fault activity area does not extend further to the southeast, Daofu and points south may become an earthquake danger zone. Topographic observation must be stepped up in this region and in an area north of Danba.

AUTHOR: JING Beike [2529 0554 4430]

ORG: None

TITLE: "Shifts in the Foci of Strong Earthquakes"

SOURCE: Beijing DIZHEN ZHANXIAN [SEISMOLOGY FRONT] in Chinese No 2, 26 Mar 80 pp 10-11, 18

ABSTRACT: Movement of the foci of successive earthquakes was plotted against time in three major earthquake belts in China: the Qilingshan-Liupanshan Fold System Earthquake Belt, the North-South Earthquake Belt and the Shanxi Uplift Region Subsidence Earthquake Belt. In all cases, significant linear plots were obtained. In the case of the North-South Belt, a reversal of the direction of shifting of the earthquake foci was noted in the late 1960's; in the case of the Shanxi Uplift Region belt two separate shift patterns occurring simultaneously were identified. The blocks at whose junctions earthquakes occur turn relative to one another, and when an earthquake on one section of the junction produces fracturing, the section where accumulated stress exists to be released in an earthquake moves down the junction.

AUTHOR: GAO Jizeng [7559 4949 1350]

ORG: None

TITLE: "Geothermal Anomalies"

SOURCE: Beijing DIZHEN ZHANXIAN [SEISMOLOGY FRONT] in Chinese No 2, 26 Mar 80 pp 12-13, 20

ABSTRACT: Regions in which the ground temperature gradient or the heat flux density are higher (or lower) than average are geothermal anomalies. These areas are found in association with earthquake zones worldwide, and in China (Taiwan hot springs areas, Tibet and Yunnan in the Mediterranean-Himalaya belt). The principal reason is that faulting associated with earthquakes also provides passages for upward movement of heat from the deeper regions of the earth. A table showing earthquake frequencies for 3 geothermal fields in China is presented. Eight geothermal phenomena associated with earthquakes are identified: appearance of warm springs, increasing temperature of warm springs, sudden changes in ground temperature, issuing of steam from the ground, hot steam geysers from holes and fissures, issuing of sulfur-containing gases form the ground, water- or steam-related "explosions," and local climatic warming.

AUTHORS: LIU Yuansheng [0491 0337 3932], ZOU Quansheng [6760 2164 3932], Li Jinquan [2621 6855 2164], ZHANG Tianqing [1728 1131 1987]

ORG: None

TITLE: "Changes in Oil Well Output Related to Earthquakes"

SOURCE: Beijing DIZHEN ZHANXIAN [SEISMOLOGY FRONT] in Chinese No 2, 26 Mar 80 pp 17-18

ABSTRACT: Before the 9 June 1979 Bohai earthquake (magnitude 4.0), an increase in oil output from well No S-265 in the vicinity of the earthquake area had been noticed. Thereafter, output of this well was monitored carefully, and another sudden increase in output was noted on 29 June, which was followed by another earthquake of magnitude 4.0 the following day. In both cases the jump in production was pronounced, in one case increasing from about 40 to about 80 tons per day in the course of 2 days (output had been abnormally low--15 tons a day--rather more than a week before), and on the second occasion rising from the vicinity of 50 tons a day to 75 and 78 tons a day in the course of 2 days. In the Shengli oilfield, two wells (Nos S-513 and S-111) also showed extremely large jumps in output a few days before the 1976 Tangshan earthquake.

AUTHORS: TANG Xinzhong [0781 5281 0022], BAO Hongru [7637 3163 0320]

ORG: None

TITLE: "Earthquakes and Changes in Gases in Underground Water"

SOURCE: Beijing DIZHEN ZHANXIAN [SEISMOLOGY FRONT] in Chinese No 2, 26 Mar 80 pp 21-22, 45

ABSTRACT: Gases dissolved in water were measured in a number of wells starting in 1974. Initially a chemical adsorption method was used to determine total gases, carbon dioxide and oxygen; starting in November 1975 the gas chromatographic method was used to determine carbon dioxide, oxygen, nitrogen, methane and total gases. Pronounced changes in total gas content in the water of the Mian No 4 well were found starting in January 1976, presumably associated with the August 1976 Tangshan earthquake. The Jing No 2 well showed changes in carbon dioxide and total gases which may have been associated with the 15 November 1976 and 12 May 1977 Ninghe earthquakes, but it is important to recognize the factors which can cause fluctuation in the readings and render the data invalid. Three of these factors are considered: changes in sampling conditions (in particular changes in the depth from which the sample is pumped), temperature at which the gases are extracted (i.e. in colder in situ conditions or in warmer laboratory conditions), and variations in the efficiency of extraction of the gases from the water.

AUTHOR: WU Shuqi [0702 2885 3823]

ORG: None

TITLE: "Trends in Earthquake Prediction Research"

SOURCE: Beijing DIZHEN ZHANXIAN [SEISMOLOGY FRONT] in Chinese No 2, 26 Mar 80 pp 43-45; adapted from KAGAKU [SCIENCE] in Japanese No 5, 1979

Abstract: In recent years there has been considerable progress in long-term earthquake forecasting, but less progress has been made in the important areas of mid-term and short-term forecasting. An important contribution to earthquake theory has been the dilatancy theory, which holds that before earthquakes small fractures appear in rock, causing it to expand, after which water enters the fissures, ultimately leading to failure and an earthquake. This theory explains phenomena such as ground swelling, the speed of earthquake waves, radon content of subsurface water and electrical resistivity changes, but it has failed to square with more recent data. However, it has had the beneficial effect of focusing attention on a number of factors that previously had received insufficient attention. Detailed measurement of microseisms is very important because it gives detailed information on the speeds of propagation of seismic waves at different points and makes possible 3-dimensional structural diagrams which can be used in earthquake prediction, especially for the recognition of foreshocks. A block diagram showing the interrelations of various areas of earthquake prediction is presented; fault modeling, microseism data and investigation of the causes of stress accumulation are the basis of a better knowledge of foreshocks and thus can contribute to short term prediction.

8480
CSO: 4009

AUTHOR: SUN Xinhua [1327 2450 5478]

ORG: None

TITLE: "Braving Wind and Waves on a Journey to the Distant Horizon"

SOURCE: Beijing JIANCHUAN ZHISHI [KNOWLEDGE OF SHIPS] in Chinese No 6, 1980 pp 2-3

ABSTRACT: As part of a Chinese delivery rocket test, a convoy of 18 ships made a 35-day, 10,000-mile cruise to the target area in the South Pacific. The 18 ships included guided missile destroyer No 131, Xiangyanghong No 5, Yuanwang No 1 and ship No 107, as well as an oil and water ship. The force was seen off in late April by Wang Zhen, Geng Biao and other civil and military dignitaries. A refueling operation was carried out en route. Other countries sent ships and aircraft to observe the results of the missile test, and the task force had to warn these out of the impact area in a peaceable manner. The instrument package ejected when the missile nose cone fell into the sea was recovered by a diver descending from a helicopter. The returning force was inspected by Ye Jianying and Zhang Aiping, and later command personnel were present in Beijing at a celebration of the successful test, attended by Hua Guofeng, Deng Xiaoping, Li Xiannian and Chen Yunfu.

AUTHOR: HAI Liu [3189 3177]

ORG: None

TITLE: "A 'Secret Weapon' and the Defense Against It"

SOURCE: Beijing JIANCHUAN ZHISHI [KNOWLEDGE OF SHIPS] in Chinese No 6, 1980 pp 12-13

ABSTRACT: Hitler's attempt to cut England's commercial lifeline in World War II took first the form of submarine warfare, then that of mining territorial waters with a new type of mine, the magnetic induction mine. These mines took a heavy toll until British scientists were able to obtain and analyze one. Since these mines were detonated by the magnetism of ship hulls, there were two ways of combat them: to detonate them by generating strong magnetic fields, and to demagnetize ship hulls. Hull demagnetization was first done by equipping the ships with a loop of wire through which current could be passed. This took up virtually all the British wire output. Later it was found that hulls could be demagnetized by passing a loop of wire around them, passing a strong pulse of current through the wire, then removing it; the demagnetization had to be repeated periodically. Demagnetization was especially important for smaller ships, and it had a critical impact on the war effort, since the evacuation from Dunkirk was done largely with small craft.

8480
CSO: 4009

END

END OF FICHE DATE FILMED

6 Jan 1981

DD.